CHIRAL MAGNETIC EFFECT &
RELATIVISTIC ISOBAR COLLISIONS

徐浩洁（HAOJIE XU）

湖州师范学院（HUZHOU UNIVERSITY）

IN COLLABORATION WITH:

LIE-WEN CHEN, YICHENG FENG, HANLIN LI, ZIWEI LIN, CAIWAN SHEN, FUQIANG WANG, XIAOBAO WANG, HANZHONG ZHANG, JIE ZHAO, YING ZHOU.

中国科学技术大学粒子物理与原子核物理学科学术报告

2022.05.06

Outline

I. Introduction

II. Search for the CME with the spectator/participant plane method

III. Search for the CME with Relativistic isobar collisions

IV. Probing the neutron structure with relativistic isobaric collisions

V. Summary

Based on: 1710.03086, 1710.07265, 1808.06711, 1808.00133, 1910.02896, 1910.06170, 2002.05220, 2103.05595, 2105.04052, 2106.15595, 2111.14812, 2204.02387

I. Introduction

Relativistic heavy ion collisions

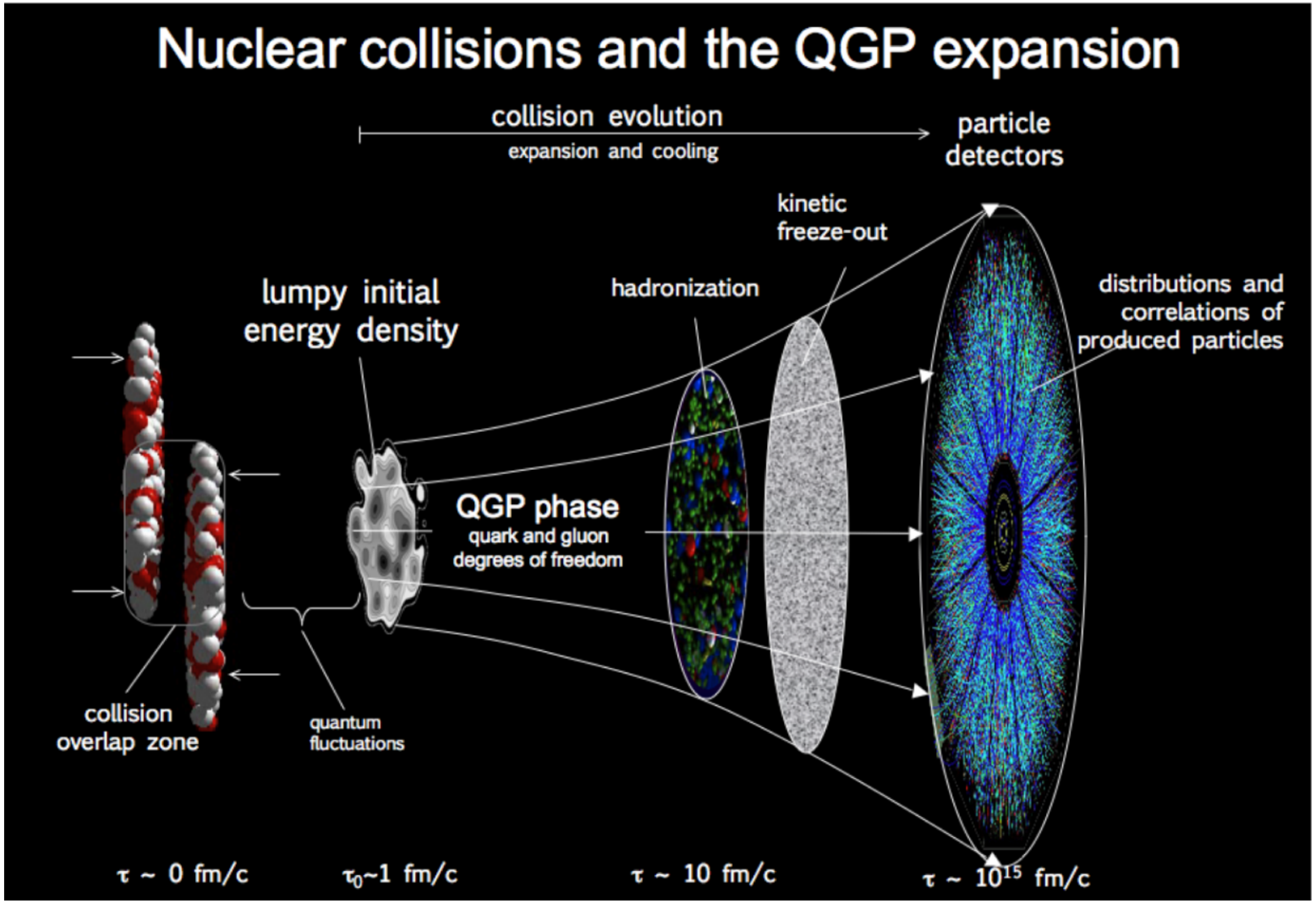

Chiral Magnetic Effect

D.E. Kharzeev et al. / Nuclear Physics A 803 (2008) 227–253

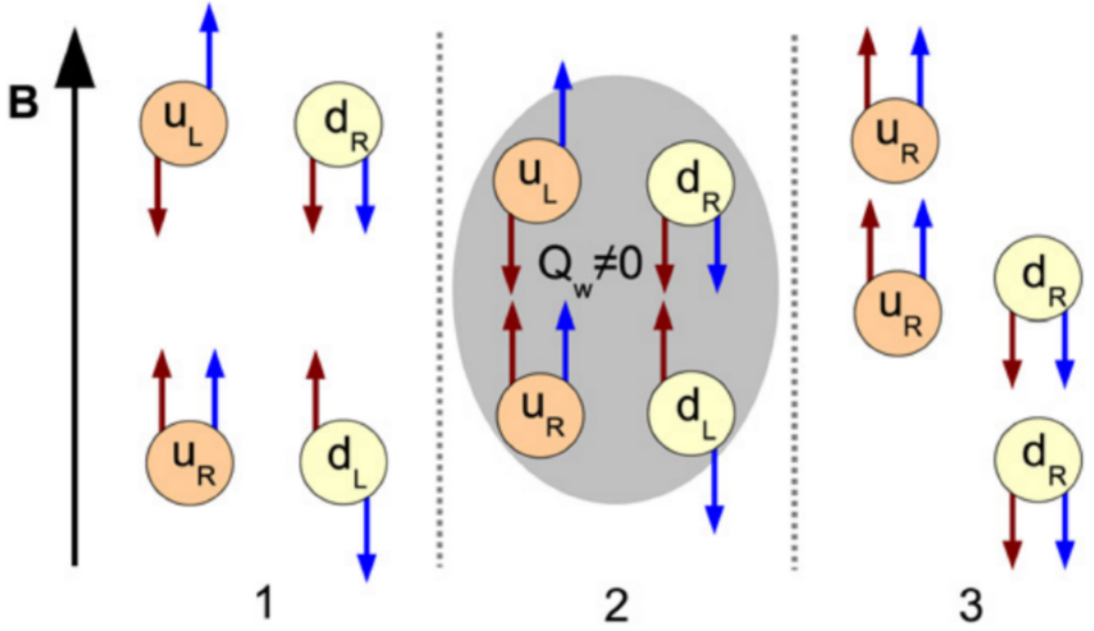

$$\mathbf{J}_{\mathbf{cme}} = \sigma_5 \mathbf{B} = \left(\frac{(Qe)^2}{2\pi^2} \mu_5 \right) \mathbf{B},$$

D. Kharzeev, PPNP88, 1(2016)

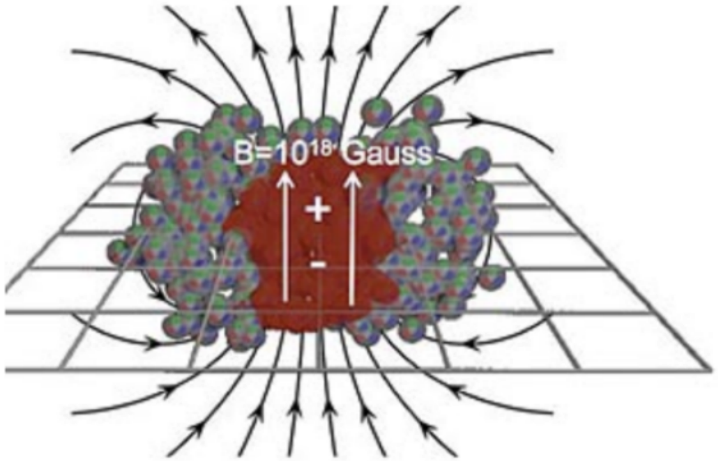

$$eB \sim m_\pi^2$$

- Magnetic field

$$Q_w = \frac{g^2}{32\pi^2} \int d^4x \, F^a_{\mu\nu} \tilde{F}^{\mu\nu}_a$$

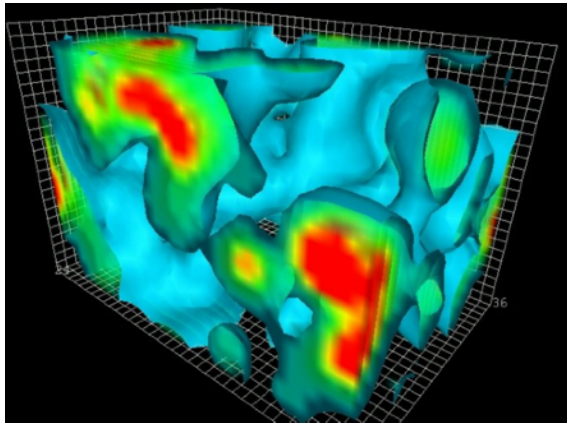

- QCD Vacuum: Fluctuations of topological charge

The gamma correlator

The gamma correlator: EBE charge separation wrt. reaction plane

$$\frac{dN_\pm}{d\phi} \propto 1 + 2v_1\cos(\phi-\Psi_{\mathrm{RP}}) + 2v_2\cos[2(\phi-\Psi_{\mathrm{RP}})] + ... + 2a_\pm\sin(\phi-\Psi_{\mathrm{RP}}) + ...,$$

$$\begin{aligned}\gamma \equiv \langle\cos(\phi_\alpha+\phi_\beta-2\Psi_{\mathrm{RP}})\rangle &= \langle\cos\Delta\phi_\alpha\ \cos\Delta\phi_\beta\rangle - \langle\sin\Delta\phi_\alpha\ \sin\Delta\phi_\beta\rangle \\ &= [\langle v_{1,\alpha}v_{1,\beta}\rangle + B_{\mathrm{IN}}] - [\langle a_\alpha a_\beta\rangle + B_{\mathrm{OUT}}] \\ &\approx -\langle a_\alpha a_\beta\rangle + [B_{\mathrm{IN}} - B_{\mathrm{OUT}}],\end{aligned}$$

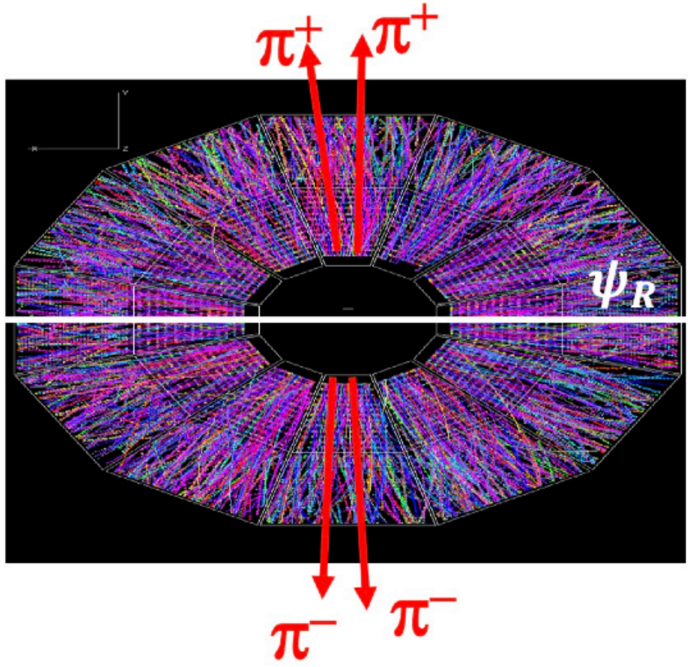

$\gamma_{+-,-+} > 0$ or $\gamma_{OS} > 0$

$\gamma_{++,--} < 0$ or $\gamma_{SS} < 0$

$\Delta\gamma > \equiv \gamma_{OS} - \gamma_{SS} > 0$

Experimental measurements

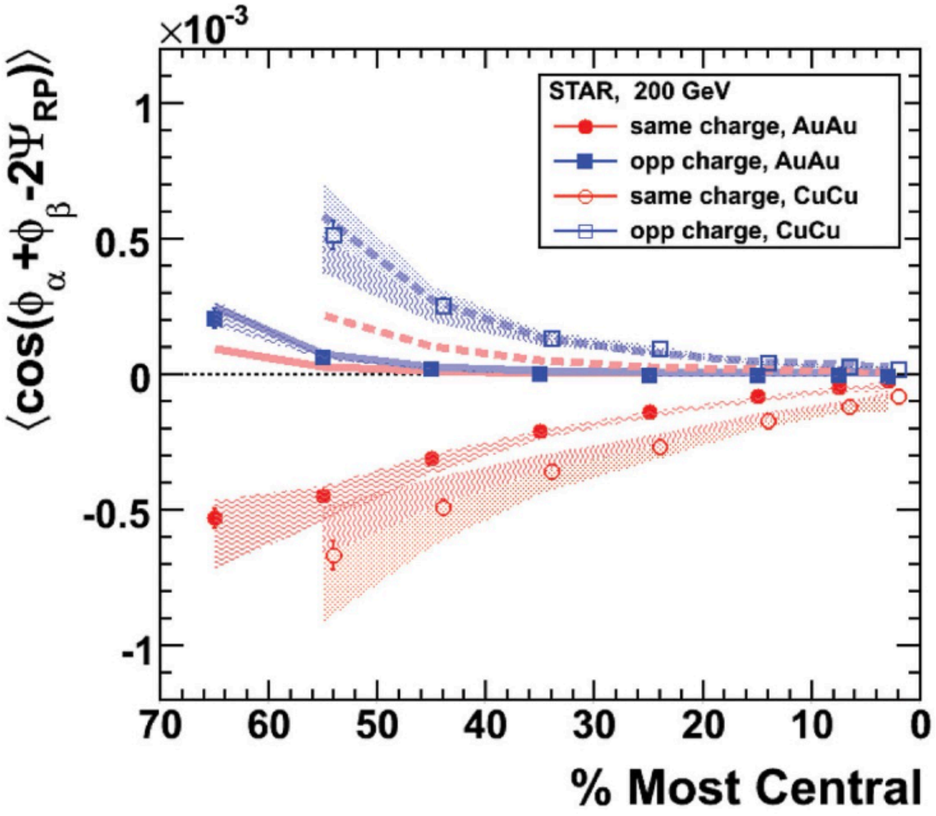

STAR, PRL103, 251601 (2009)

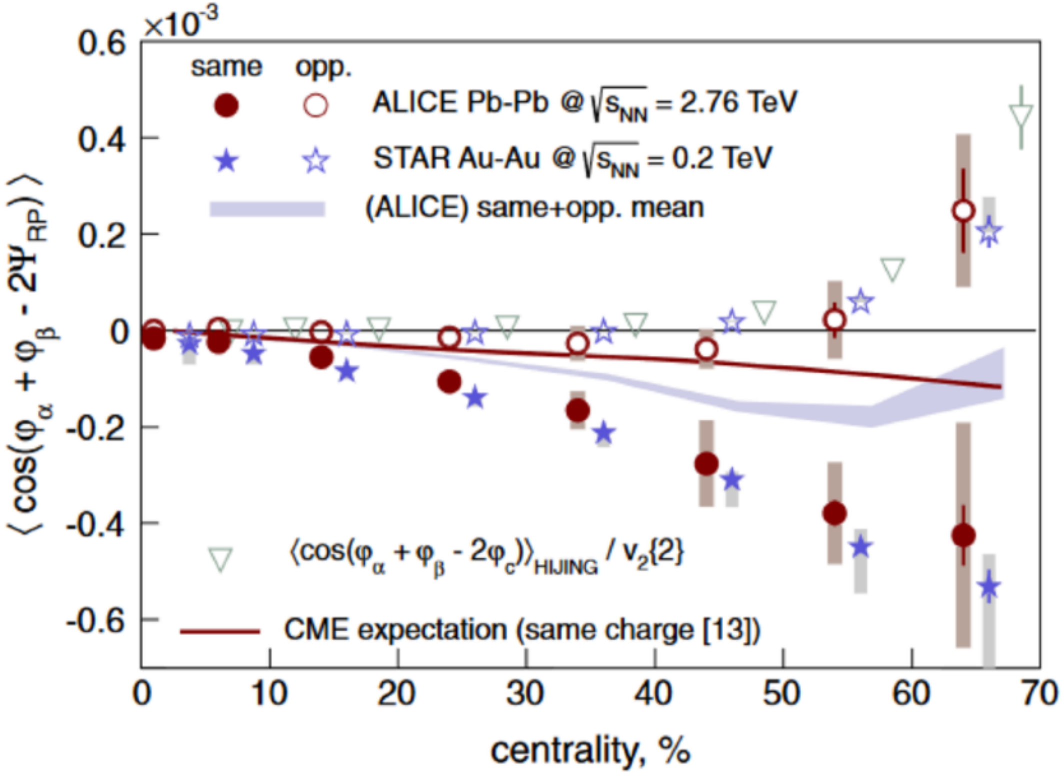

ALICE, PRL110, 012301(2013)

A clear signal compatible with EBE charge separation wrt. reaction plane is observed. However…..

Background issues

Schlichting, PRC83(2011)
Bzdak, PRC81(2010)
Wang, PRC81(2010)

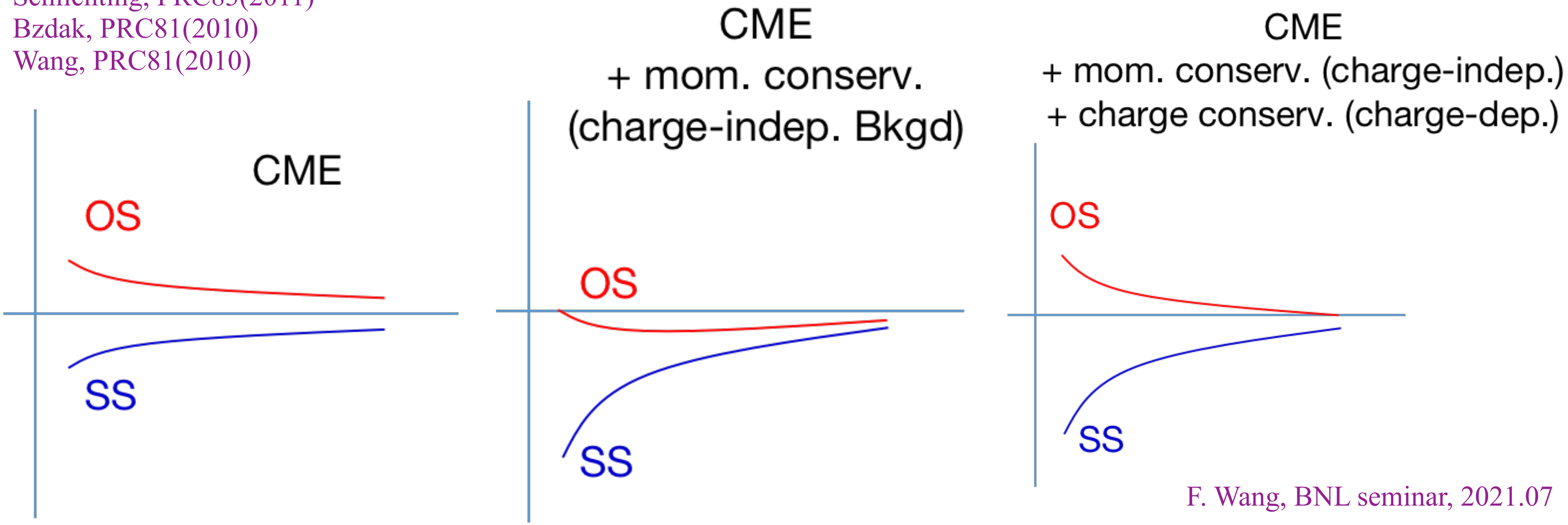

F. Wang, BNL seminar, 2021.07

$$\Delta\gamma = \gamma_{\mathrm{OS}} - \gamma_{\mathrm{SS}}$$

- Momentum conservation: charge-independent background, same contributions for γ_{OS} and γ_{SS}.
- Charge conservations: change-dependent background, can not be removed with $\Delta\gamma$

Charge conservation

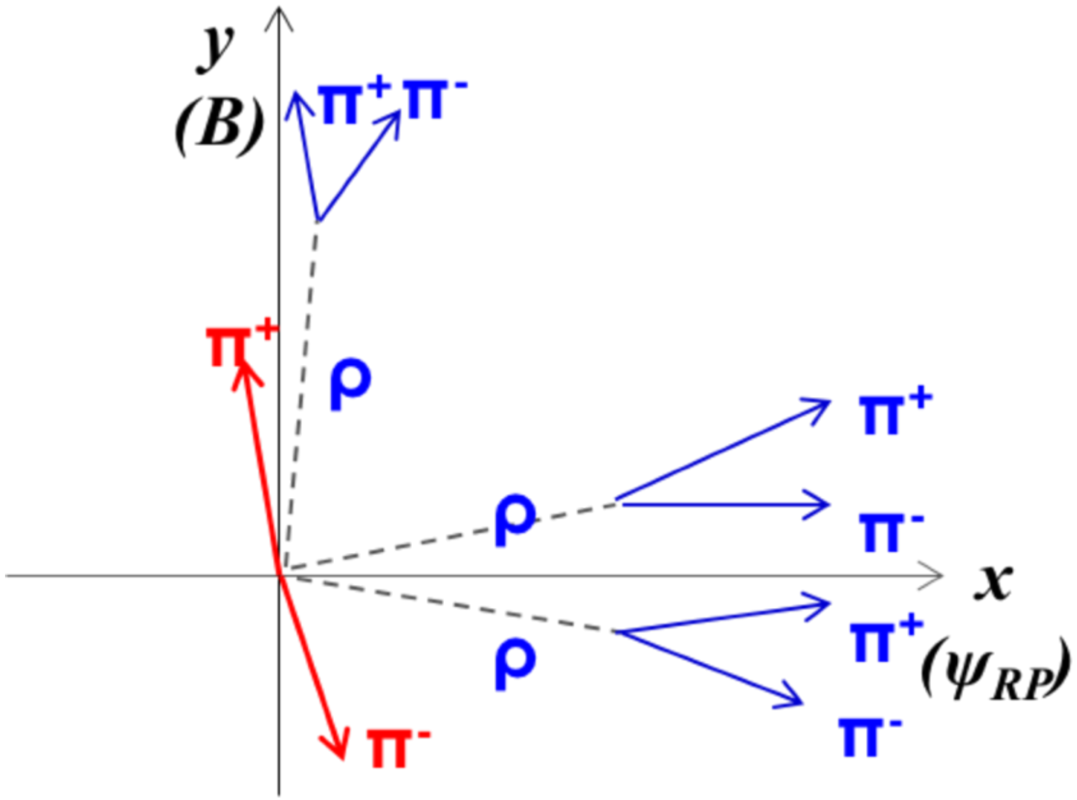

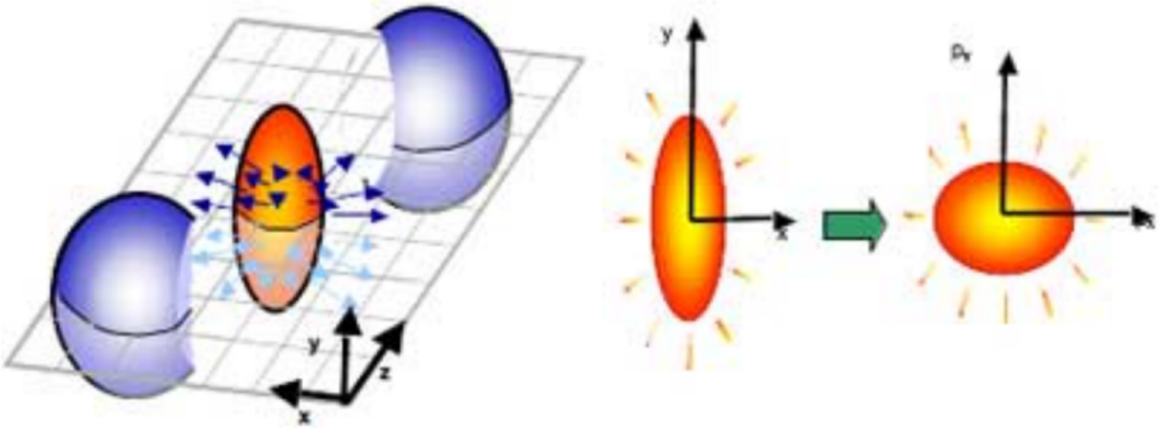

$$\frac{dN}{d\varphi} = N(1 + 2\sum_n v_n cos[n(\varphi - \Psi_n])$$

$v_2 = \langle cos2(\varphi - \Psi_2)\rangle$: elliptic flow

$$\Delta\gamma_{\mathrm{bkg}} = \langle\cos(\varphi_\alpha + \varphi_\beta - 2\Psi_{RP})\rangle = \frac{N_{\mathrm{cluster}}}{N_\alpha N_\beta} \times \langle\cos(\varphi_\alpha + \varphi_\beta - 2\Psi_{\mathrm{cluster}}) \times \cos(2\Psi_{\mathrm{cluster}} - 2\Psi_{RP})\rangle$$

Elliptic flow

Prefect fluid - strong coupling QGP (sQGP)

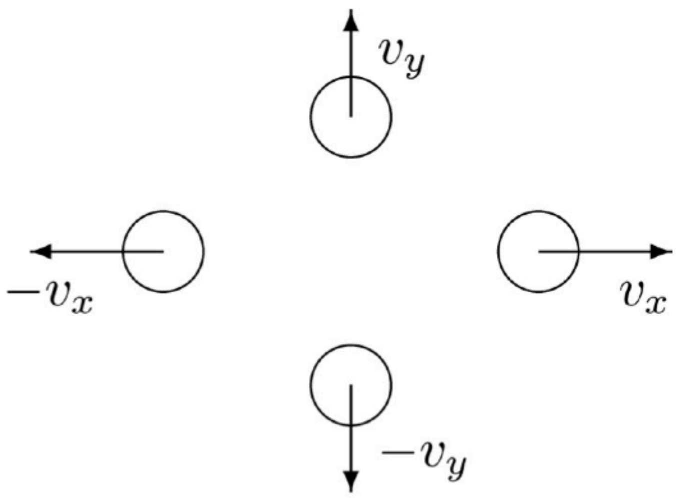

Fig. 6. Simple source of four fireballs.

$$v_2(p_t) = \frac{\int_0^{2\pi} d\phi_s \cos(2\phi_s)\, I_2(\alpha_t(\phi_s))\, K_1(\beta_t(\phi_s))}{\int_0^{2\pi} d\phi_s\, I_0(\alpha_t(\phi_s))\, K_1(\beta_t(\phi_s))}.$$

P. Huovinen, et al. PLB503, 58–64 (2001)

$$Q_n = \sum_{i=1}^{N} e^{in\varphi_i}$$

$$v_n\{2\} = \sqrt{\langle \frac{Q_n Q_n^* - N}{N(N-1)} \rangle}$$

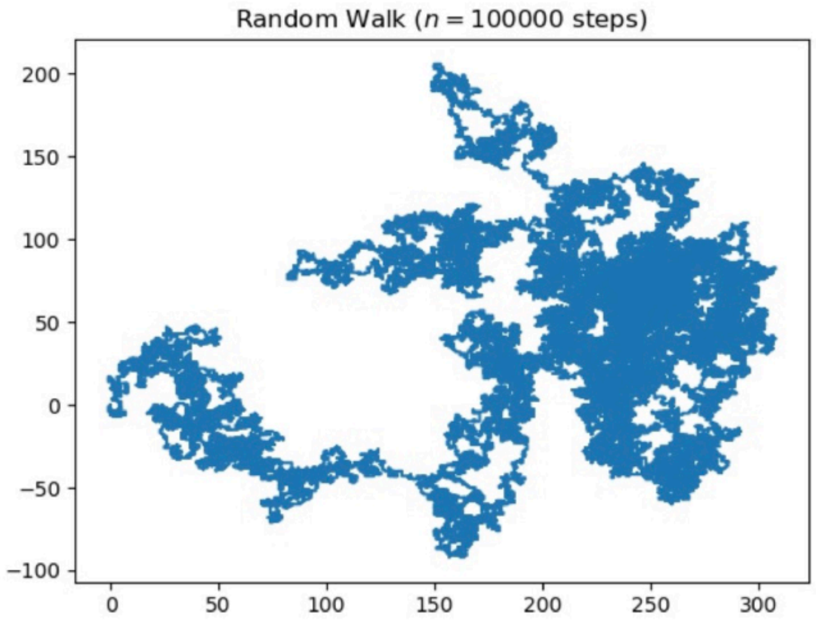

CME and background

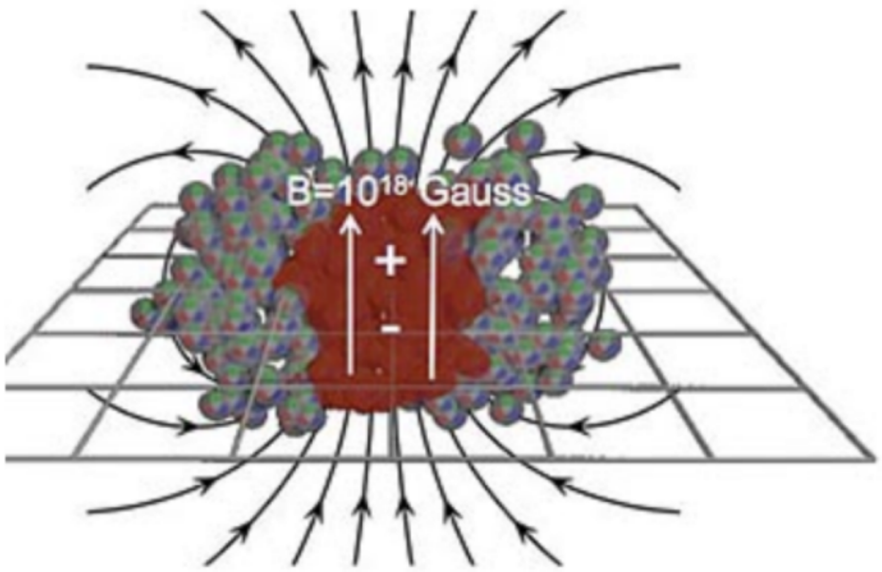

VS

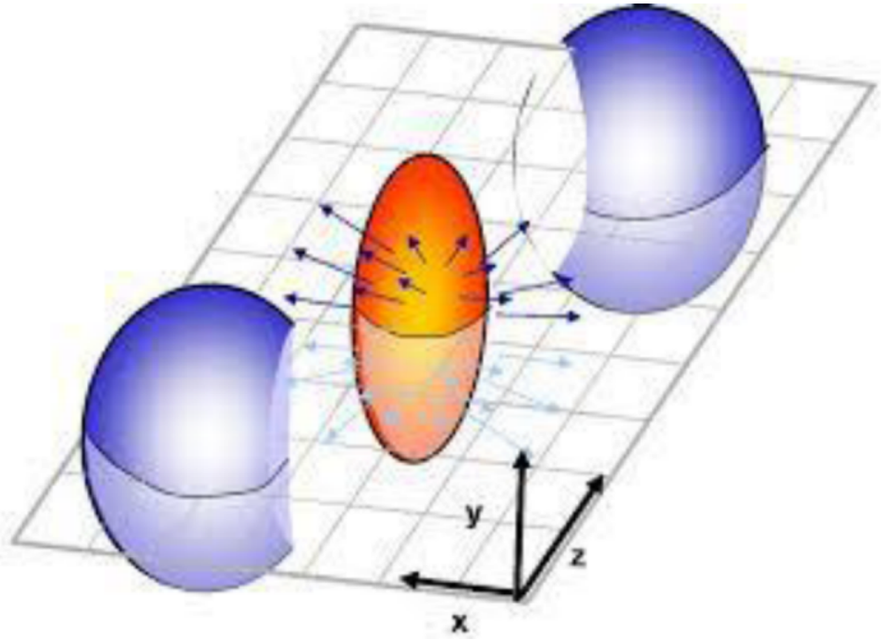

$$\mathbf{J}_{\mathbf{cme}} = \sigma_5 \mathbf{B} = \left(\frac{(Qe)^2}{2\pi^2} \mu_5 \right) \mathbf{B},$$

$$\Delta\gamma_{\mathrm{bkg}} \propto \frac{N_{\mathrm{cluster}}}{N_\alpha N_\beta} \times v_2^{\mathrm{cluster}}$$

Small system measurements

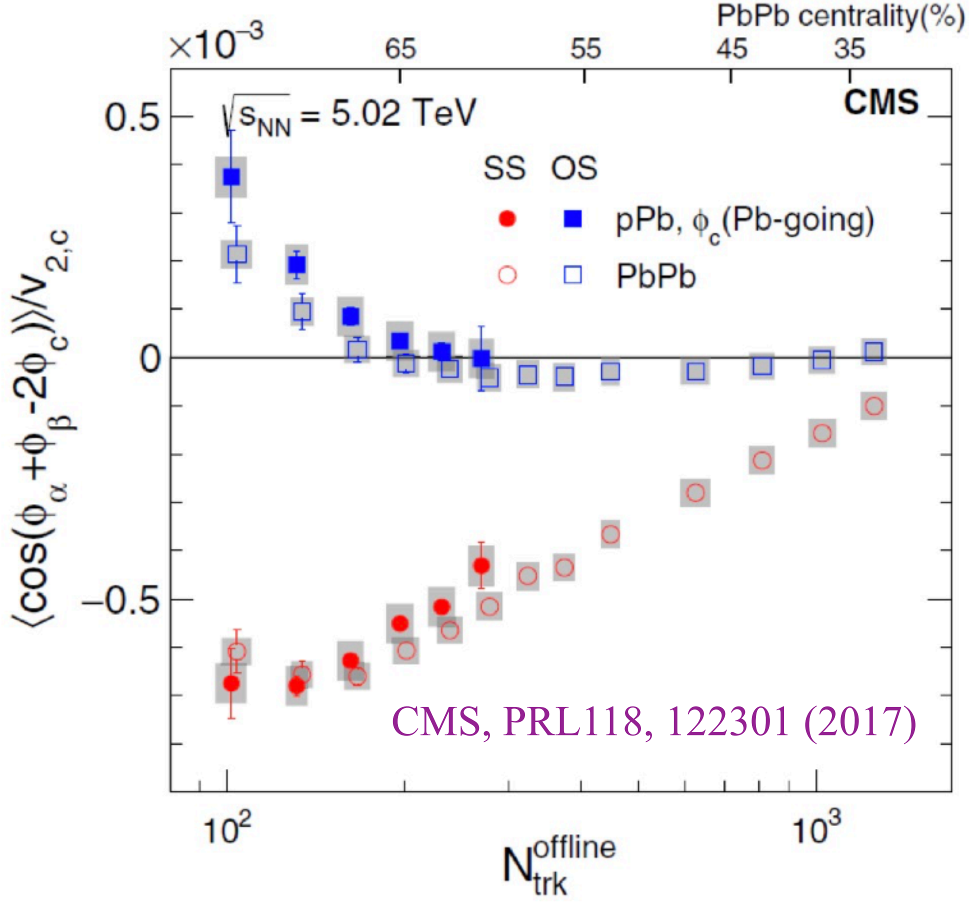

CMS, PRL118, 122301 (2017)

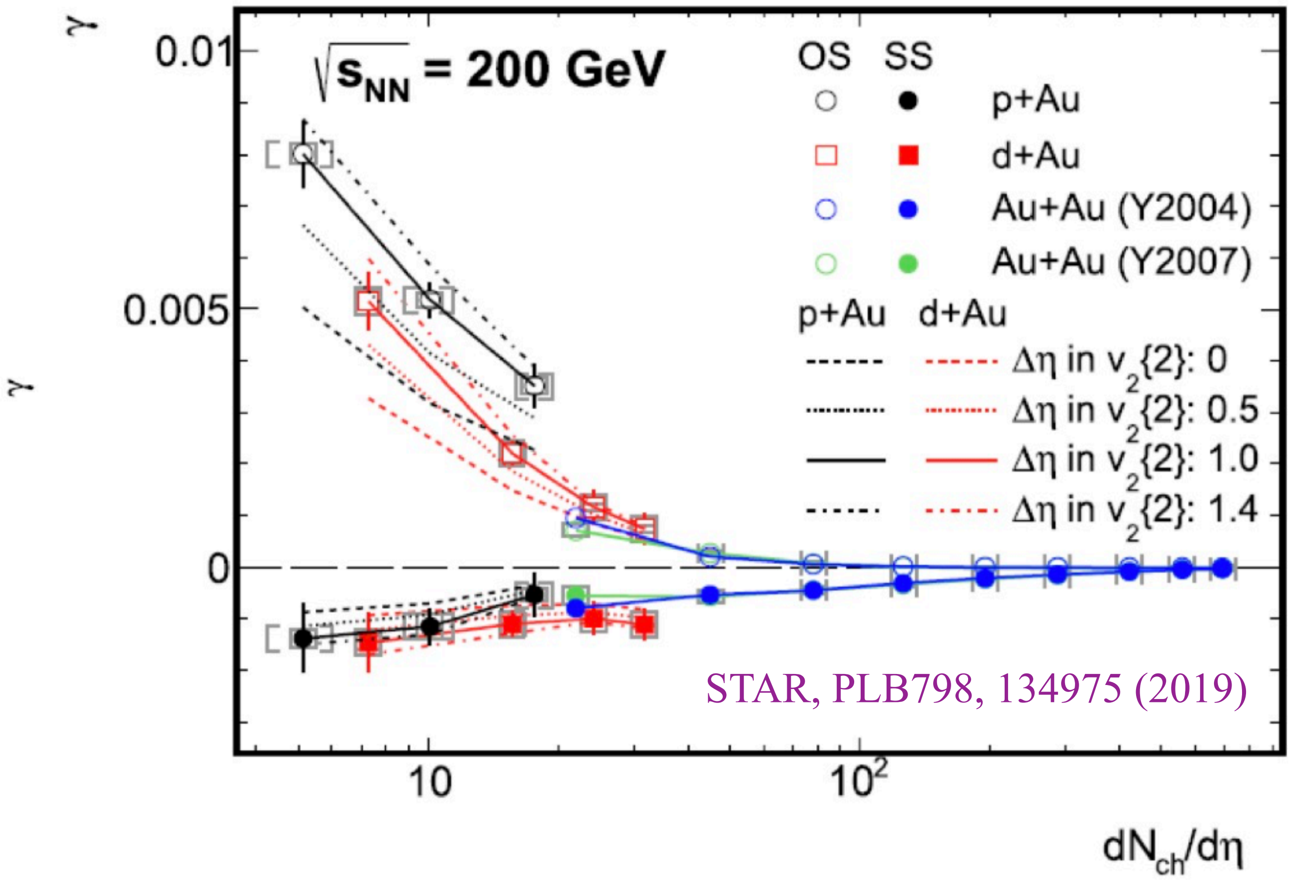

STAR, PLB798, 134975 (2019)

Large $\Delta\gamma$ in small systems indicate large background in CME measurements

II. Search for the CME with spectator/participant plane method

HJX, et al, CPC42, 084103 (2018)

SP/PP method

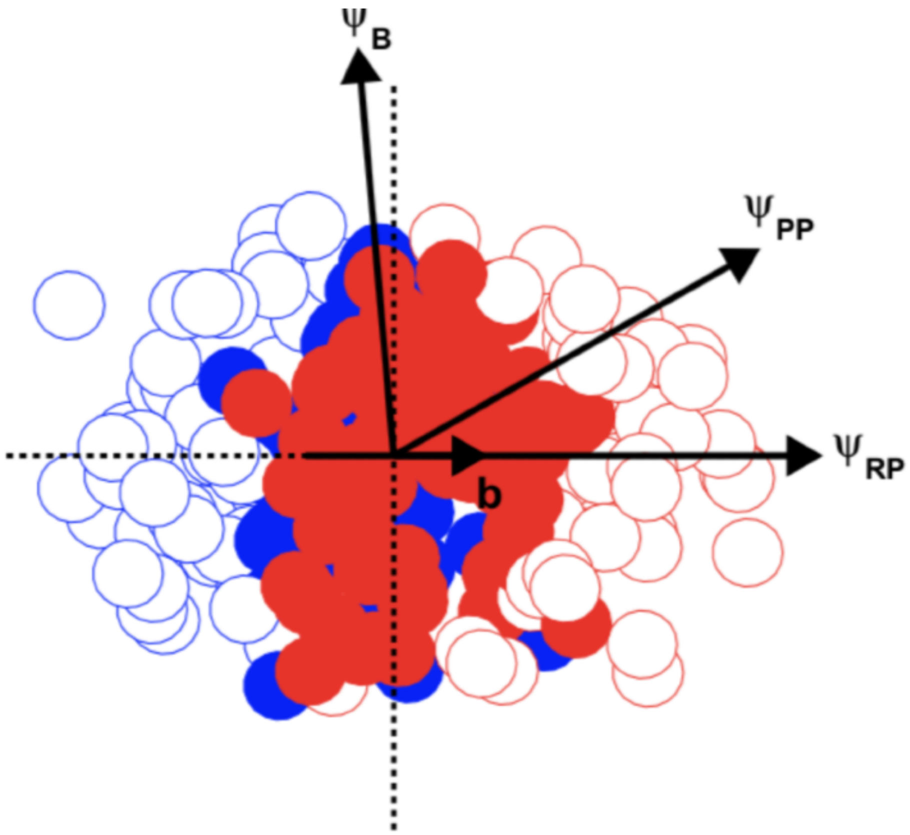

“Varying the chiral magnetic effect relative to flow in a single nucleus-nucleus collision”

Factorization

HJX, et al, CPC42, 084103 (2018)

$$a^{\rm PP}_{\epsilon_2} \equiv \epsilon_2\{\psi_{\rm RP}\}/\epsilon_2\{\psi_{\rm PP}\} \approx a^{\rm PP} ,$$

$$a^{\rm PP}_{B_{\rm sq}} \equiv B_{\rm sq}\{\psi_{\rm PP}\}/B_{\rm sq}\{\psi_{\rm RP}\} \approx a^{\rm PP} .$$

where $a^{\rm PP} \equiv \langle\cos 2(\psi_{\rm PP} - \psi_{\rm RP})\rangle$.

$$a^{\rm EP}_{v_2} \equiv v_2\{\psi_{\rm RP}\}/v_2\{\psi_{\rm EP}\} \approx a^{\rm EP} ,$$

$$a^{\rm EP}_{B_{\rm sq}} \equiv B_{\rm sq}\{\psi_{\rm EP}\}/B_{\rm sq}\{\psi_{\rm RP}\} \approx a^{\rm EP} .$$

where $a^{\rm EP} = \langle\cos 2(\psi_{\rm EP} - \psi_{\rm RP})\rangle/\mathcal{R}_{\rm EP}$

EM filed

$$e\mathbf{B}(t,\mathbf{r}) = \frac{e^2}{4\pi}\sum_n Z_n(\mathbf{R}_n)\frac{1-v_n^2}{[R_n^2-(\mathbf{R}_n\times\mathbf{v}_n)^2]^{3/2}}\mathbf{v}_n\times\mathbf{R}_n,$$

$$e\mathbf{E}(t,\mathbf{r}) = \frac{e^2}{4\pi}\sum_n Z_n(\mathbf{R}_n)\frac{1-v_n^2}{[R_n^2-(\mathbf{R}_n\times\mathbf{v}_n)^2]^{3/2}}\mathbf{R}_n, \quad (2.1)$$

Eccentricity/elliptic flow

$$\epsilon_2\{\psi_{\{PP\}}\} = \langle\frac{\langle r_\perp^2 e^{2i\phi_r}\rangle}{\langle r_\perp^2\rangle}\rangle$$

$$v_2\{\psi_{\{EP\}}\} = \langle\langle e^{2i\phi}\rangle\rangle$$

CME-v_2 filter

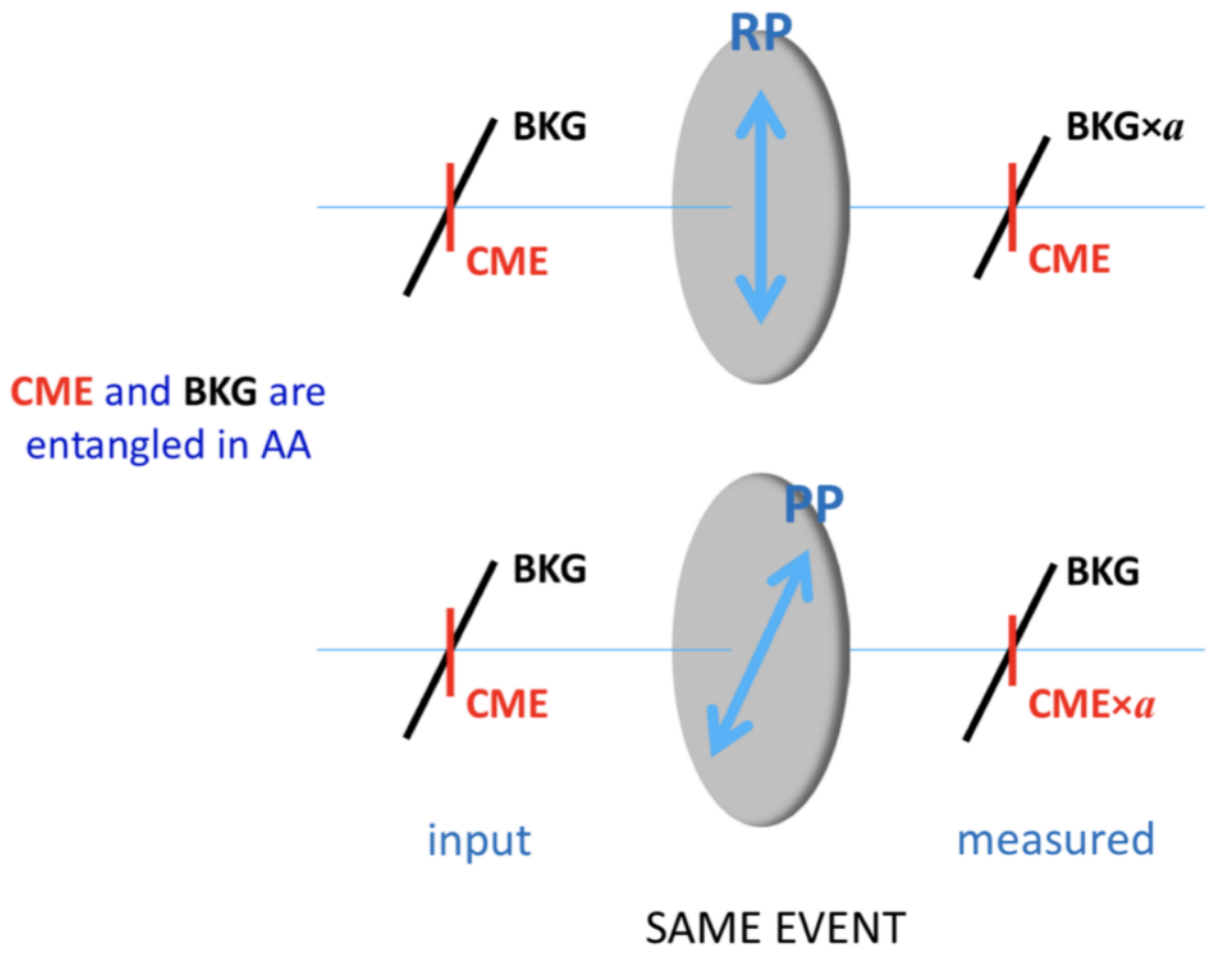

$$a \equiv \langle \cos 2(\psi_{PP} - \psi_{RP}) \rangle$$

Apply to data

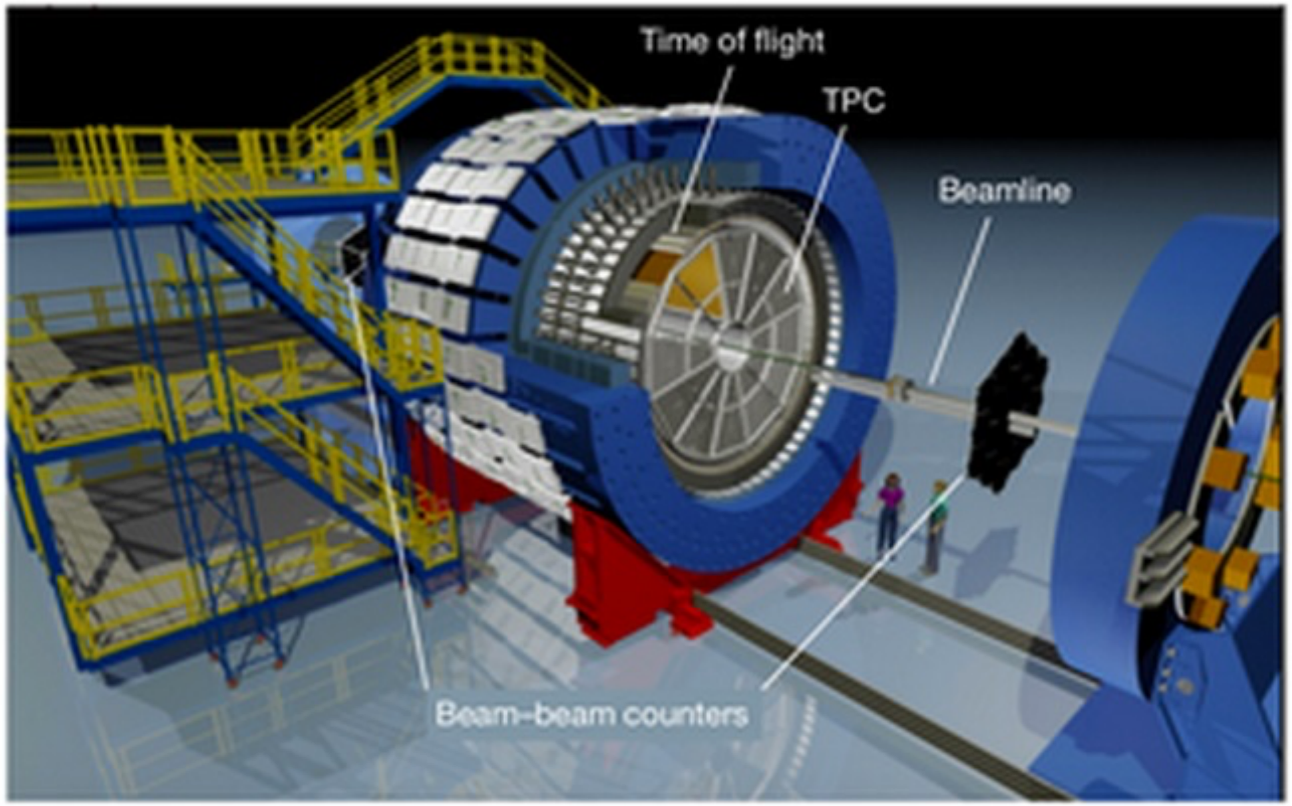

TPC: Ψ_{EP}, proxy of Ψ_{PP}
ZDC: Ψ_{ZDC}, proxy of Ψ_{SP} (Ψ_{RP})

$$f_{CME} = \frac{A/a - 1}{1/a^2 - 1}$$ where

$$A = \Delta\gamma_{ZDC}/\Delta\gamma_{TPC}$$

$$a = v_2\{\mathrm{ZDC}\}/v_2\{\mathrm{TPC}\}$$

STAR AuAu@200GeV

STAR, PRL128, 092301 (2022)

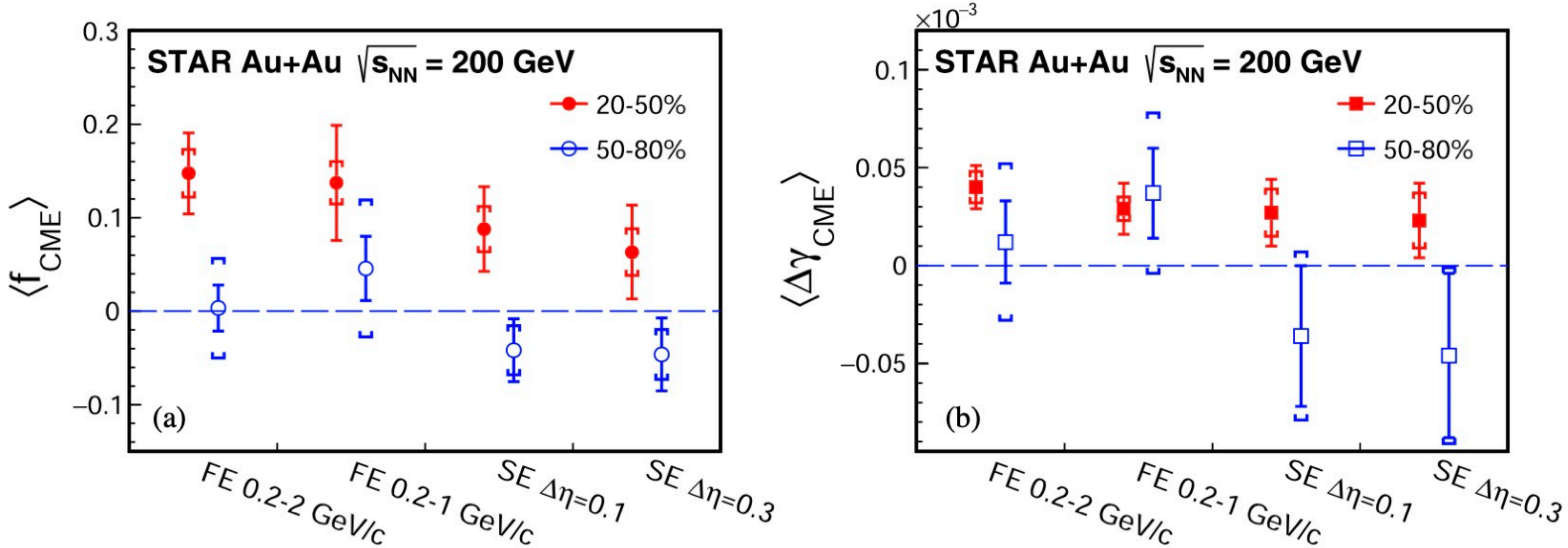

Indications of finite signal in mid-central 20-50% collisions, with 1-3σ significance (2.4B)

Expect 20B events from Run23 + Run25.

Non-flow effect

Y. Feng, et.al, PRC105, 024913 (2022)

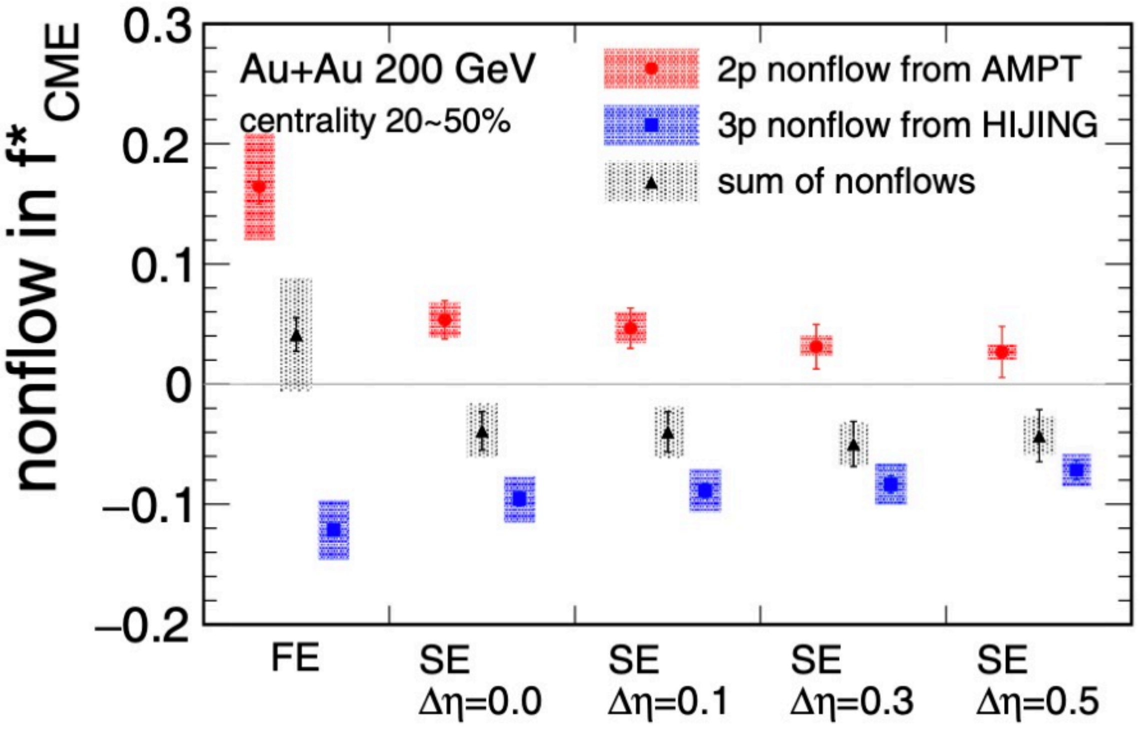

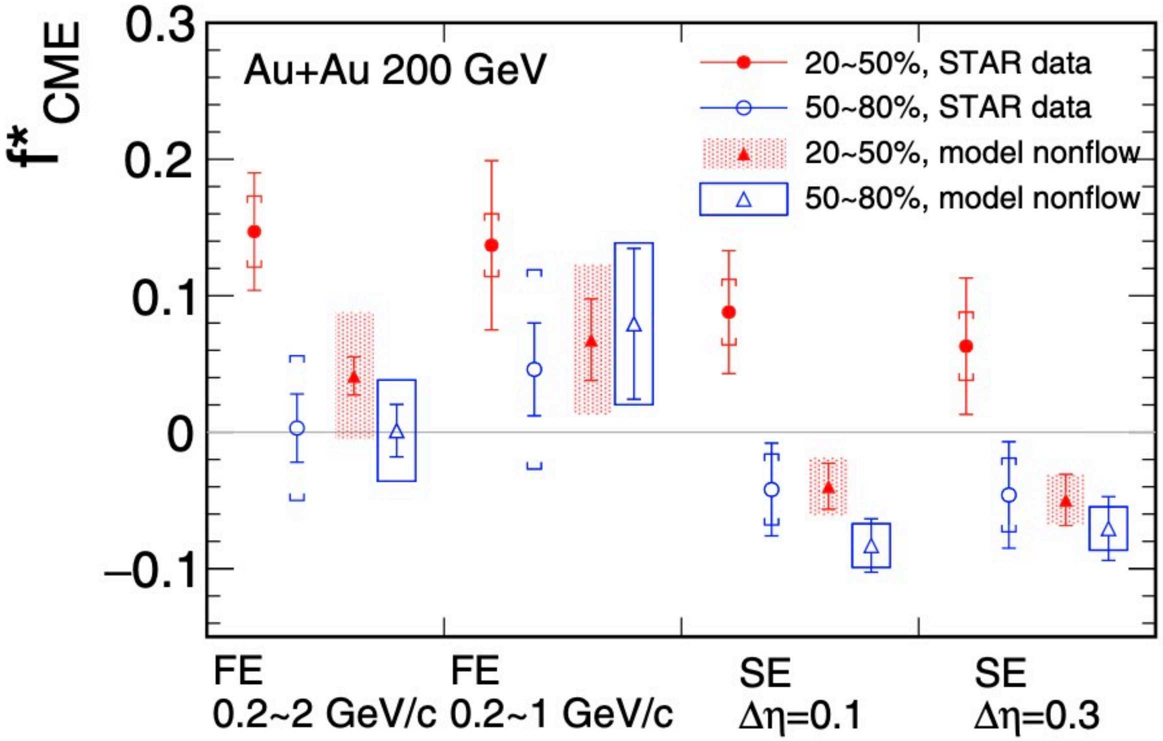

Need more rigorous non-flow studies

D. Kharzeev, PLB 633, 260 (2006)
D. Kharzeev, PRD 83, 085007 (2006)
D. Kharzeev, PPNP 88, 1 (2016)

Non-flow in CMW measurements

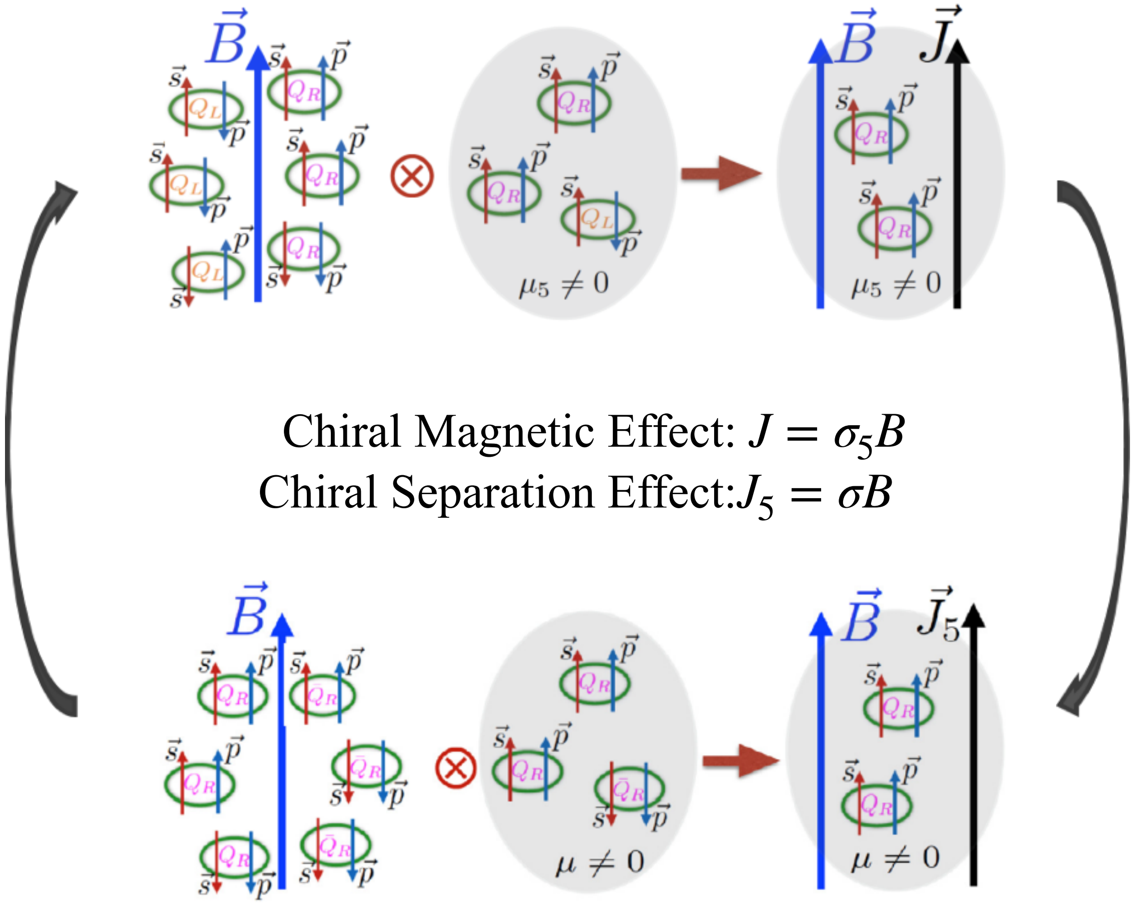

Chiral Magnetic Effect: $J = \sigma_5 B$
Chiral Separation Effect: $J_5 = \sigma B$

The Chiral Magnetic Wave (CMW) is a gapless collective excitation of the QGP stemming from the interplay of the CME and CSE

The A_{ch}-dependent ellliptic flow $v_2^{\pm} = v_2 \mp \frac{r}{2} A_{ch}$

$A_{ch} = \frac{N_+ - N_-}{N_+ + N_-}$

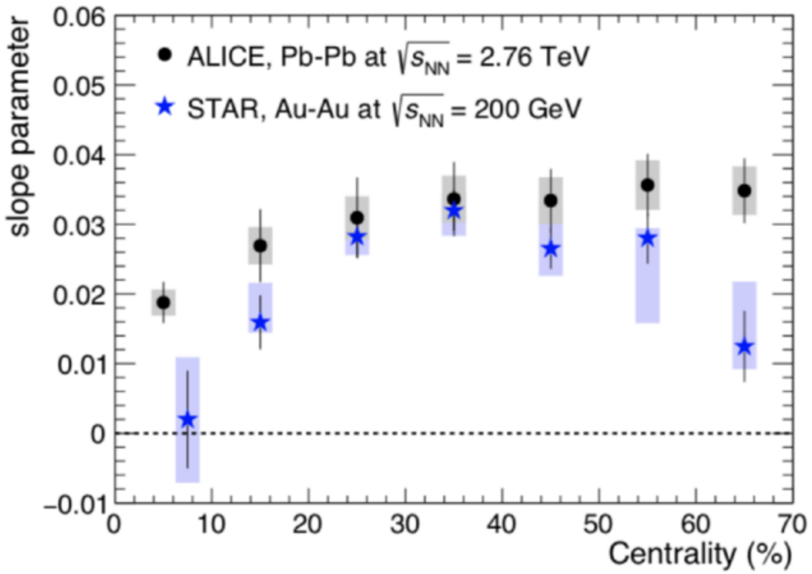

Background: Local charge conservation

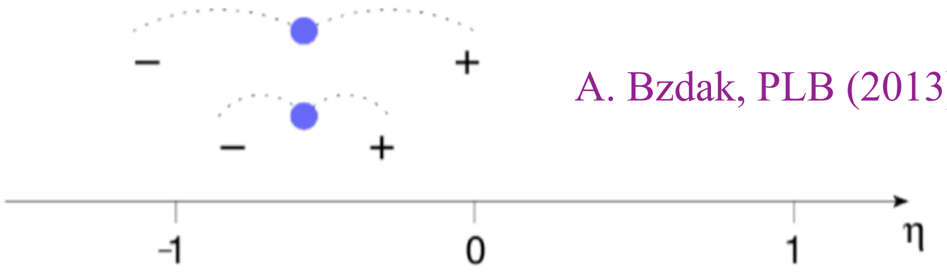

A. Bzdak, PLB (2013)

Non-flow in CMW measurements

$$d_n\{2;\pi^{\pm}h\} = \frac{d_n\{2;\pi^{\pm}h^{+}\} + d_n\{2;\pi^{\pm}h^{-}\}}{2} + \frac{d_n\{2;\pi^{\pm}h^{+}\} - d_n\{2;\pi^{\pm}h^{-}\}}{2}A_{\mathrm{ch}},$$

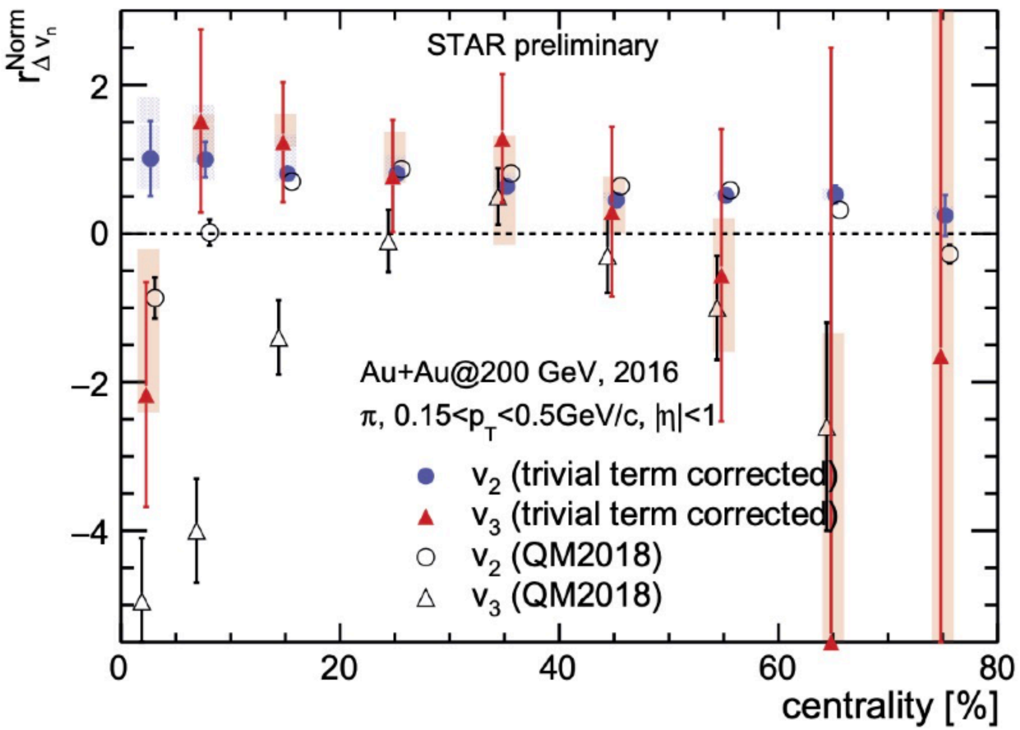

HJX, et.al, PRC101, 014913 (2020)
HJX(STAR), QM2019 poster
HJX, et.al, NPA105, 121770(2021)

The trivial term arises from non-flow differs between like-sign and unlike-sign pairs.

III. Search for the CME with Relativistic isobar collisions

Relativistic isobaric collisions

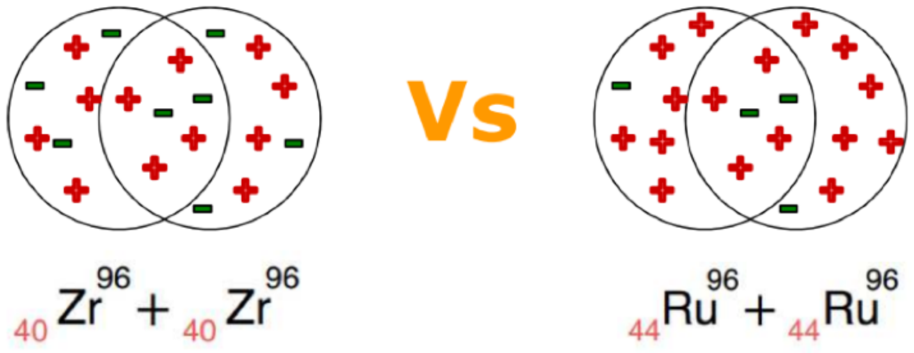

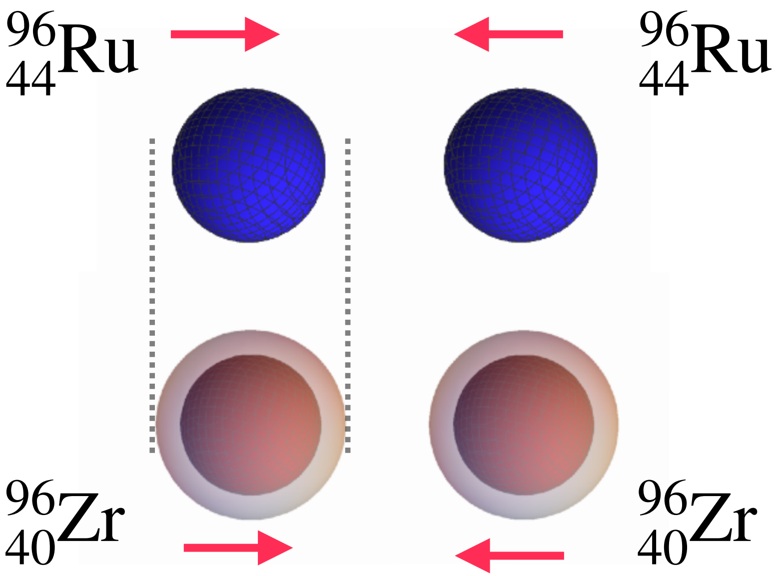

- Same multiplicity distributions, eccentricities => same background
- Different magnetic field => different CME signals

Isobar structure difference

Relativistic isobaric collisions and chiral magnetic effect

	R	a	beta2
Zr	5.02	0.46	0.08/0.217
Ru	5.085	0.46	0.158/0.053

WS parameters extracted from charge density distributions

W. Deng, X. Huang, et.al., PRC94,041901(2016)

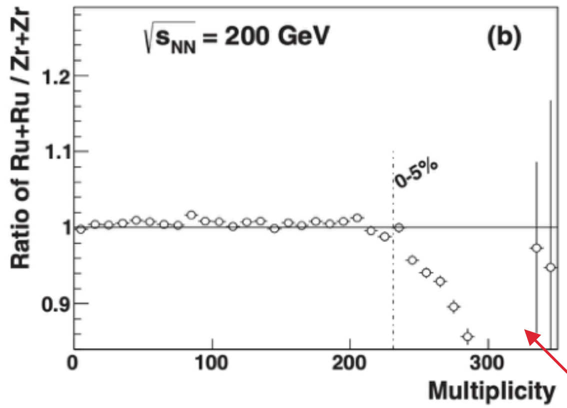

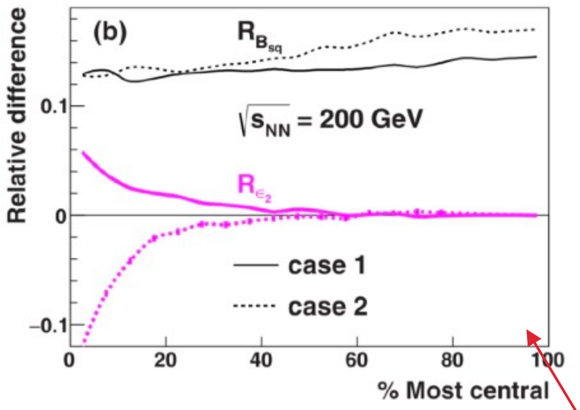

$$\Delta\gamma_{\rm bkg} = \langle\cos(\varphi_\alpha + \varphi_\beta - 2\Psi_{RP})\rangle = \frac{N_{\rm cluster}}{N_\alpha N_\beta} \times \langle\cos(\varphi_\alpha + \varphi_\beta - 2\Psi_{\rm cluster})\rangle \times v_{2,\rm cluster}$$

2010 The isobar method was proposed.
S. Voloshin, PRL105, 172301 (2010)

2016 The method was verified by model study.
W. Deng, X. Huang, et.al, PRC94, 041901 (2016)

2017 The importance of isobar structure was investigated.
HJX, et.al., PRL121, 022301 (2018)

2018 The isobar data are taken by the STAR collaboration.

2021 The first CME results published by the STAR collaboration, confirm the isobar structure differences.
STAR, PRC105, 014901 (2022)

Isobar structures are important for the CME search

STAR, Isobar, PRC105, 014901(2022)

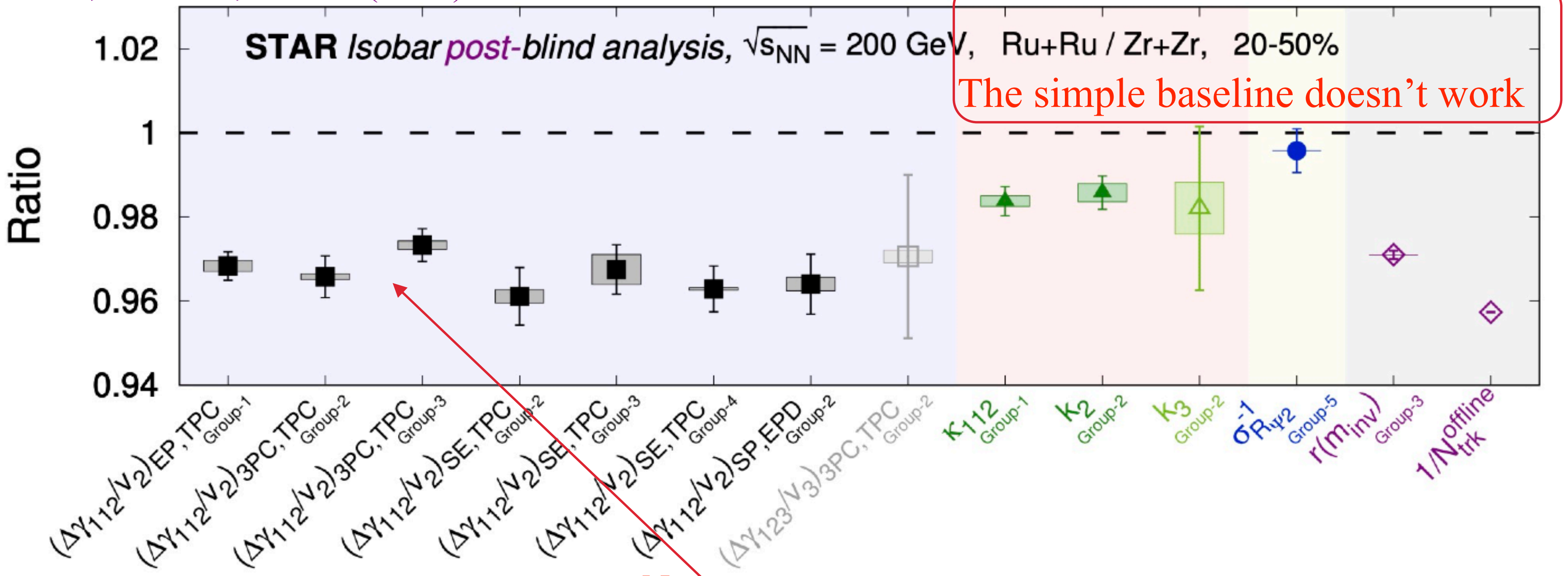

$$\Delta\gamma_{\mathrm{bkg}} = \langle\cos(\varphi_\alpha + \varphi_\beta - 2\Psi_{RP})\rangle = \frac{N_{\mathrm{cluster}}}{N_\alpha N_\beta} \times \langle\cos(\varphi_\alpha + \varphi_\beta - 2\Psi_{\mathrm{cluster}})\rangle \times v_{2,\mathrm{cluster}}$$

Multiplicity differences

Flow differences

The multiplicity and v2 differences from isobar structure are crucial for the CME search in the isobar collisions at RHIC

Neutron skin and symmetry energy

Charge density ≠ nuclear density.

Nuclear density distribution:

- Proton distribution — Can be accurately measured in experiment.
- Neutron distribution — Poorly known

Neutron skin: RMS radii differences between neutron distribution and proton distribution

$$\Delta r_{np} \equiv \sqrt{\langle r_n^2 \rangle} - \sqrt{\langle r_p^2 \rangle}$$

Neutron skin depends on symmetry energy:

$$E(\rho,\delta) = E_0(\rho) + E_{\mathrm{sym}}(\rho)\delta^2 + O(\delta^4)$$

$$\rho = \rho_n + \rho_p;\ \delta = \frac{\rho_n - \rho_p}{\rho}$$

$$L(\rho_c) = 3\rho_c \left[\frac{dE_{\mathrm{sym}}(\rho)}{d\rho}\right]_{\rho=\rho_c} ;\ \rho_c \simeq 0.11\mathrm{fm}^{-3}$$

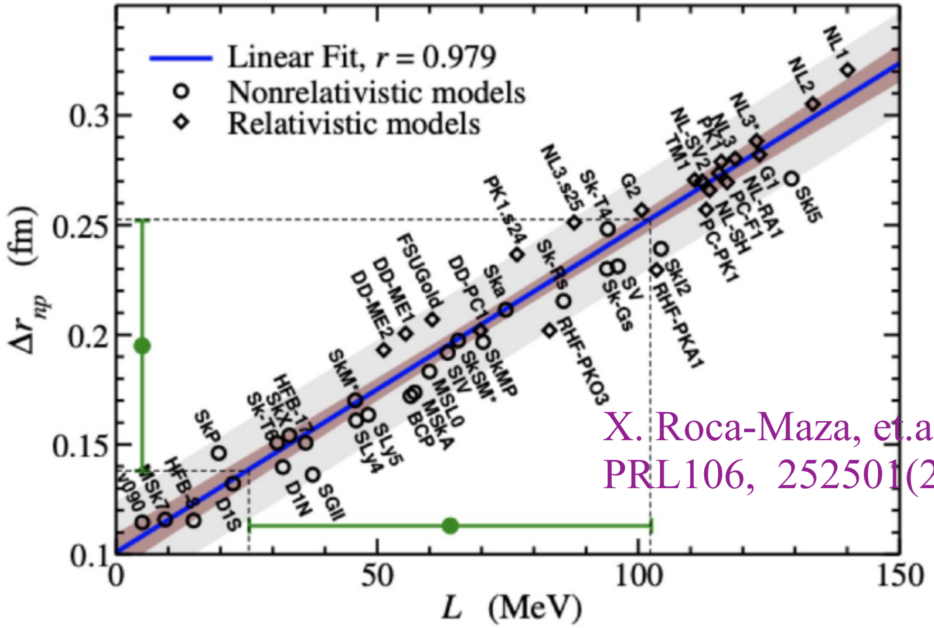

X. Roca-Maza, et.al., PRL106, 252501(2011)

The symmetry energy is crucial to our understanding of the masses and drip lines of neutron-rich nuclei and the equation of state (EOS) of nuclear and neutron star matter.

Charge densities and nuclear density in isobar collisions

- **Charge density ≠ nuclear density.**

Normally we assume neutron density profile = proton's. It's mostly ok, but for the CME search where the signal is small and we rely on large cancellation of backgrounds between two systems, we should take the difference between neutron and proton densities into consideration.

HJX, et.al., PRL121, 022301 (2018)
H. Li, HJX, et.al., PRC98, 054907(2018)

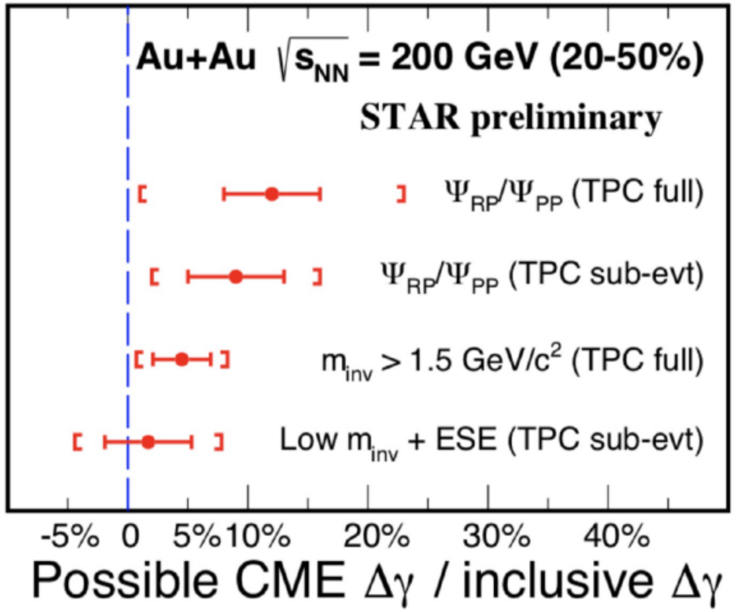

STAR Collaboration, NPA982, 535(2019)

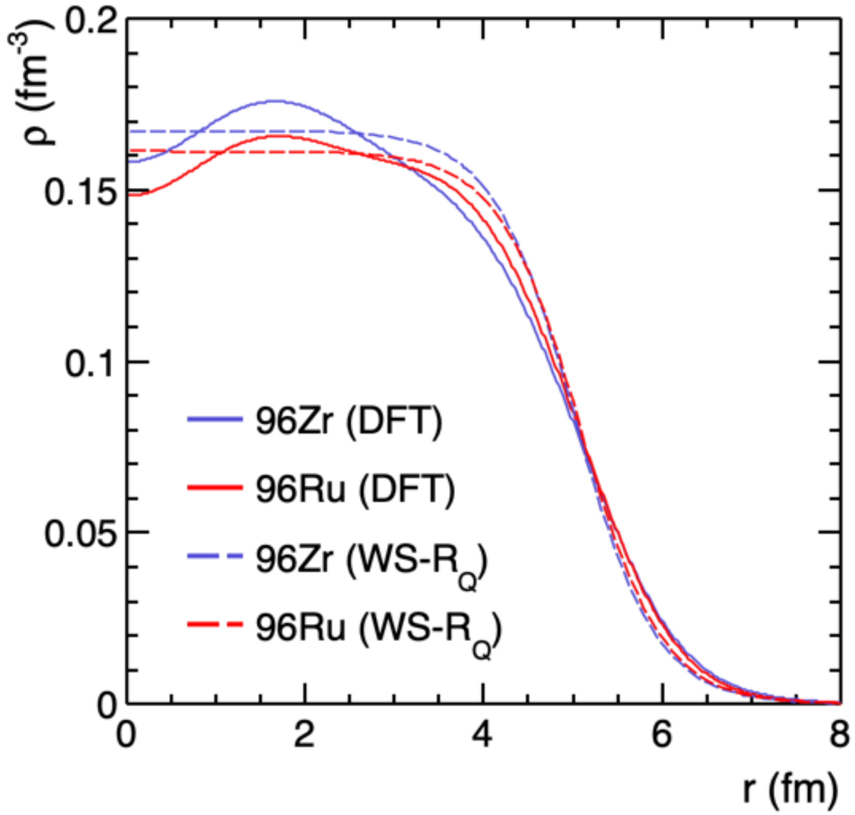

Background dominated
--- The CME signal, if exist, is very small

- Instead of the WS densities with parameters extracted from the measured charge densities, we use the proton and neutron densities obtained from the energy density functional theory (DFT) with Skyrme parameter set SLy4.

Haojie Xu

Multiplicity distribution difference between isobars

Predictions with charge densities

W. Deng, et.al., PRC94,041901(2016)

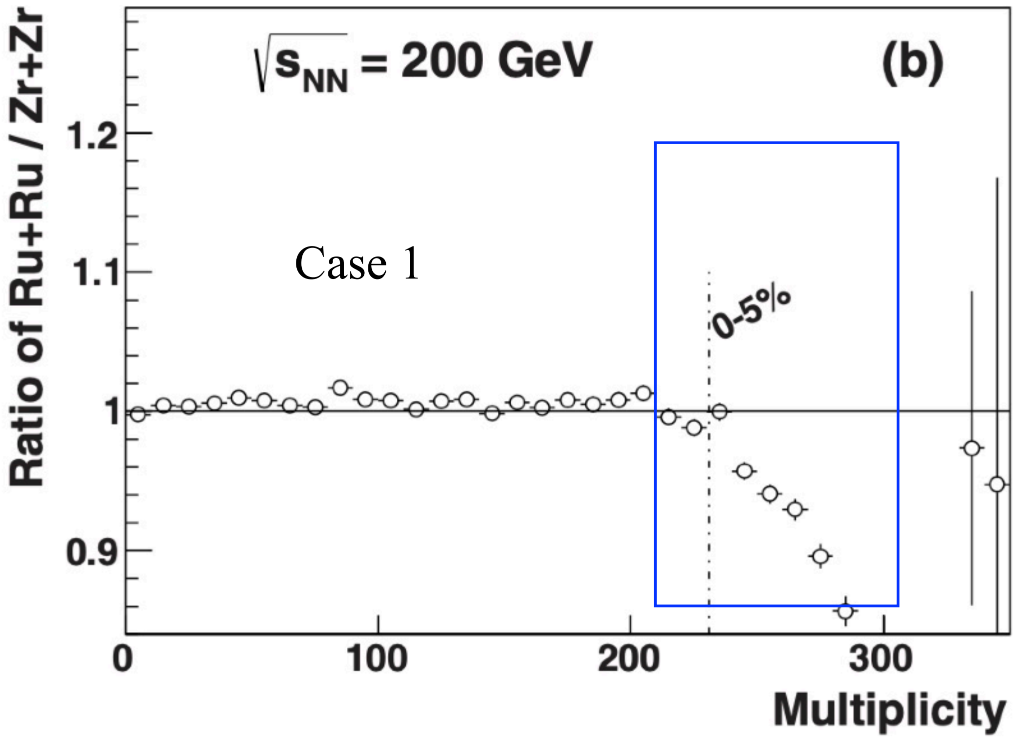

Predictions with DFT densities

H. Li, HJX, et.al., PRC98, 054907(2018)

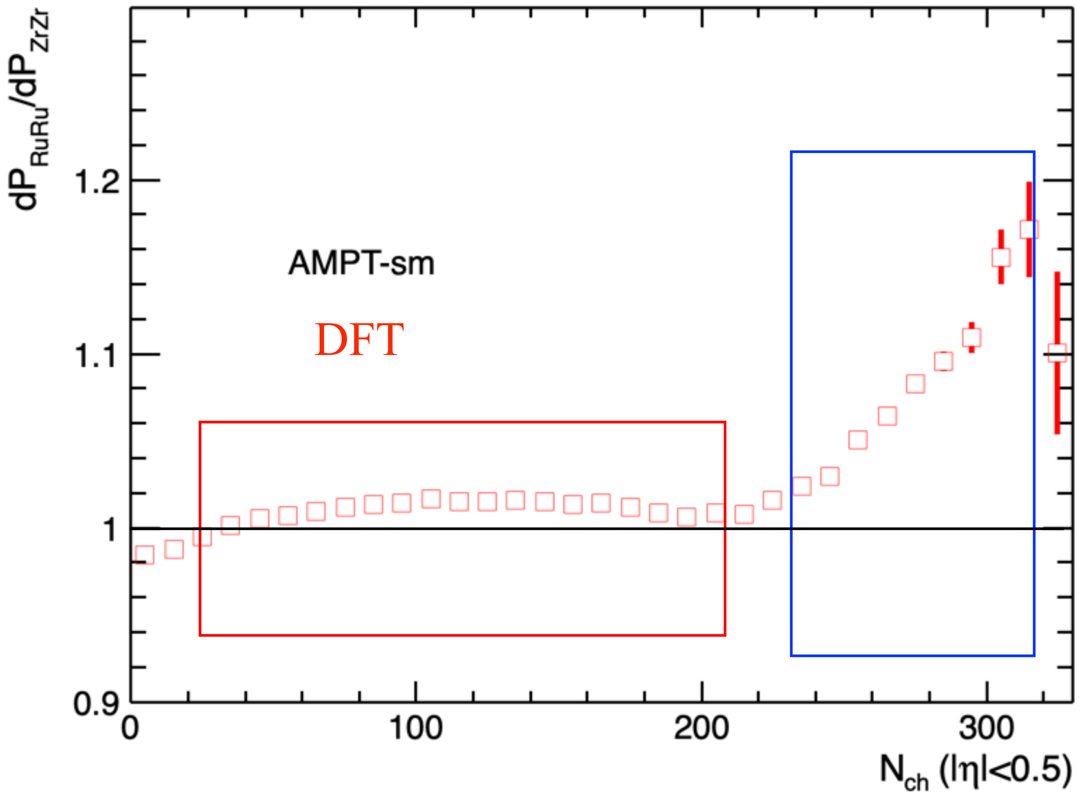

Opposite predictions from WS charge densities and DFT densities (neutron skins)

v_2 difference between isobars

Predictions from charge densities with deformation

W. Deng, et.al., PRC94,041901(2016)

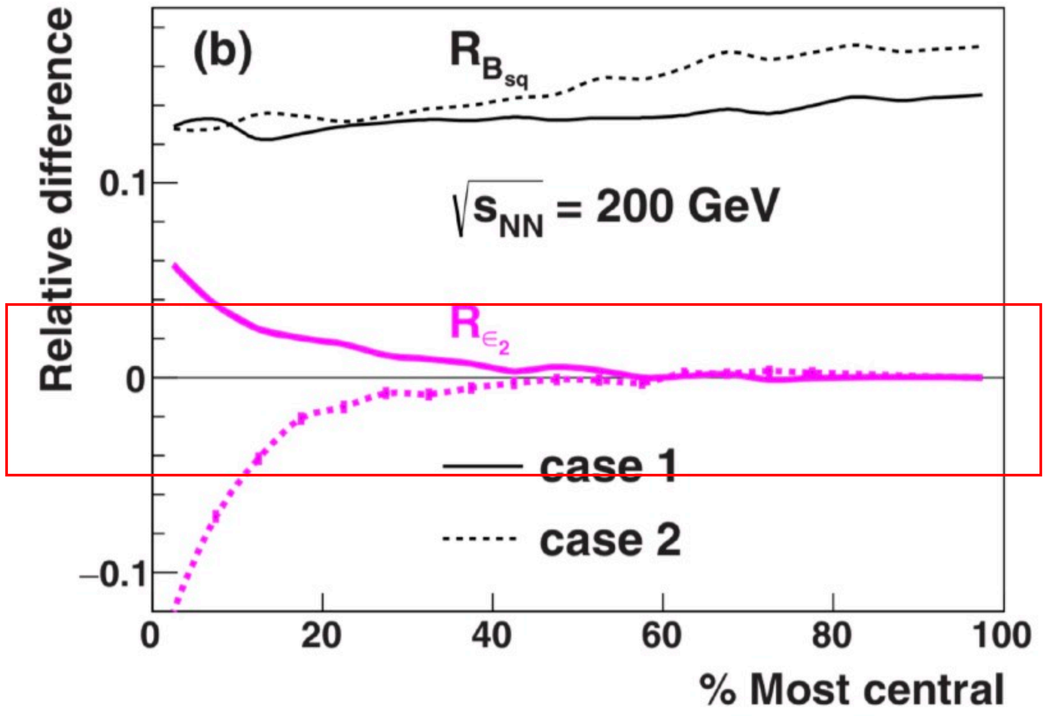

Predictions from DFT densities without deformation

HJX, et.al., PRL121, 022301 (2018)

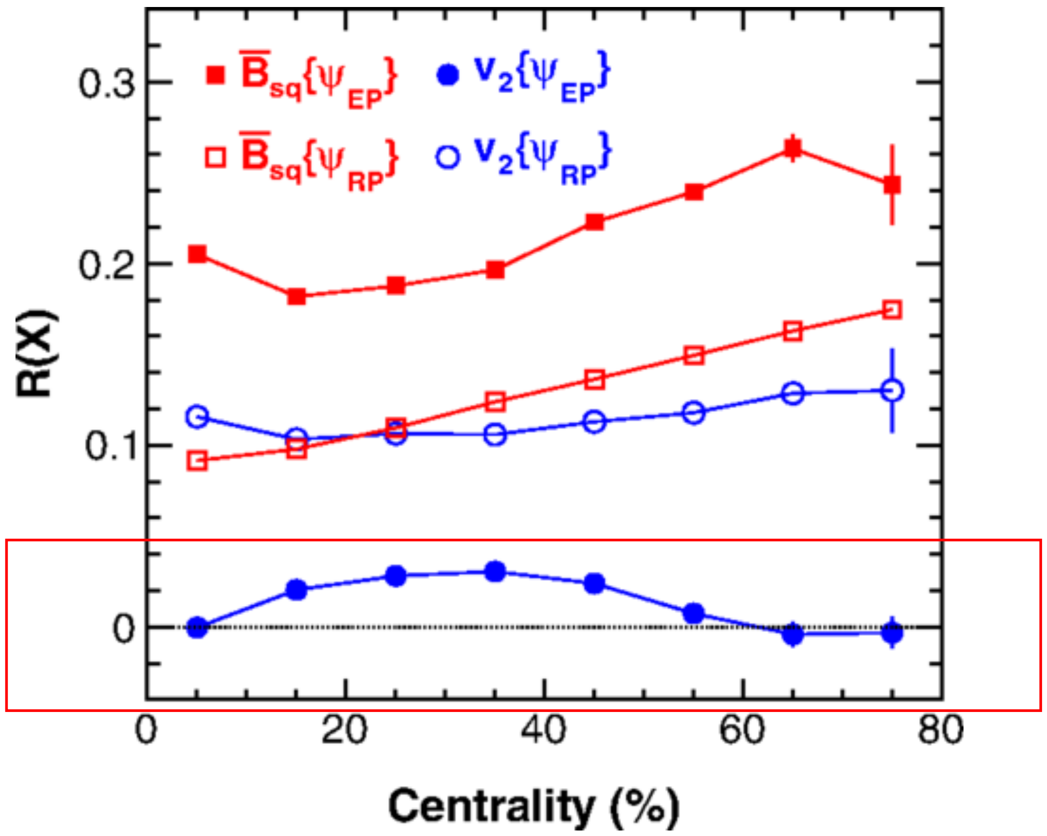

Compare to the predictions from charge densities, the calculations with DFT densities indicate that the Zr+Zr collisions and Ru+Ru collisions **have sizable differences in v_2 in 20-50% centrality range**.

Determine the neutron skin type by STAR data

HJX, et.al., PLB819, 136453 (2021)

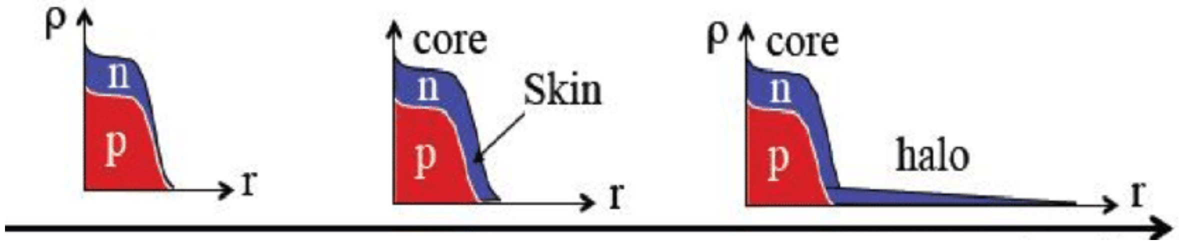

- Neutron-skin nuclei and neutron-halo nuclei for Zr

	^{96}Ru		^{96}Zr	
	R	a	R	a
p	5.085	0.523	5.021	0.523
skin-type n	5.085	0.523	5.194	0.523
halo-type n	5.085	0.523	5.021	0.592

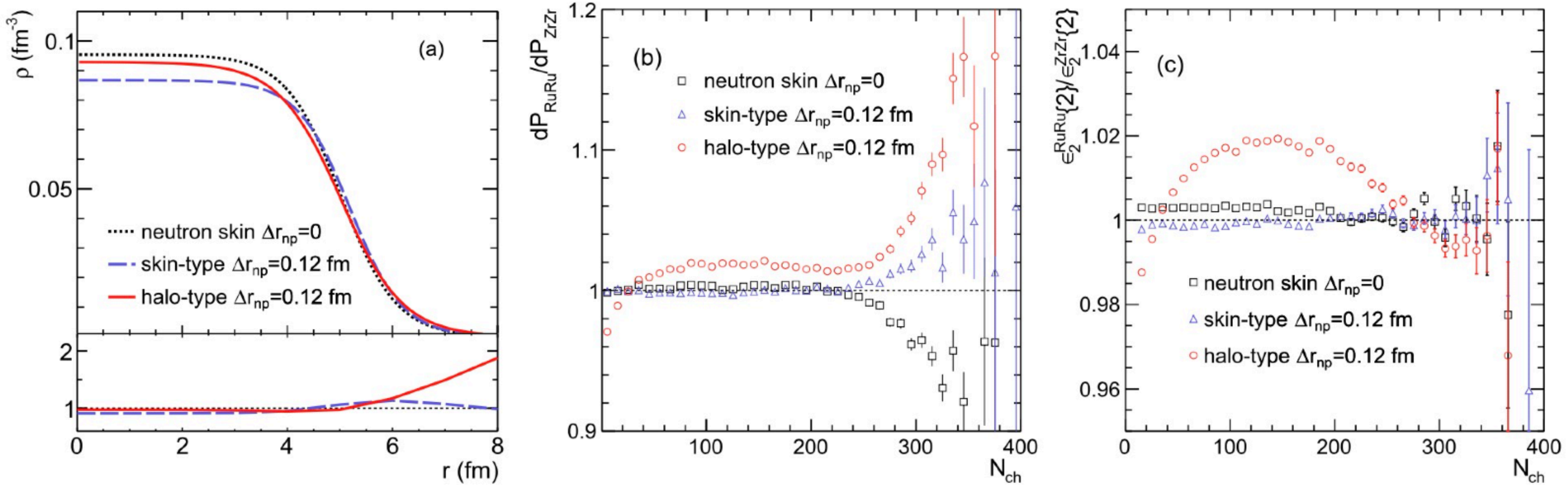

The shapes of the Ru+Ru/Zr+Zr ratios of the multiplicity and eccentricity in mid-central collisions can further distinguish between skin-type and halo-type neutron densities.

DFT predictions are verified by STAR data

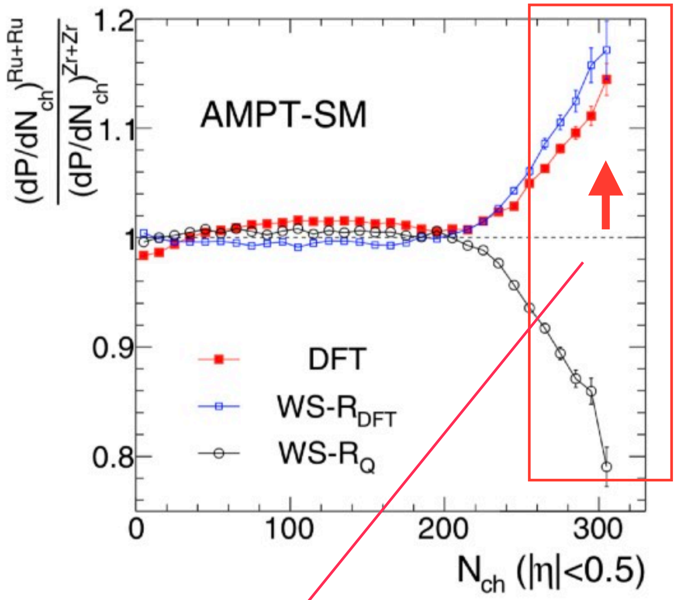

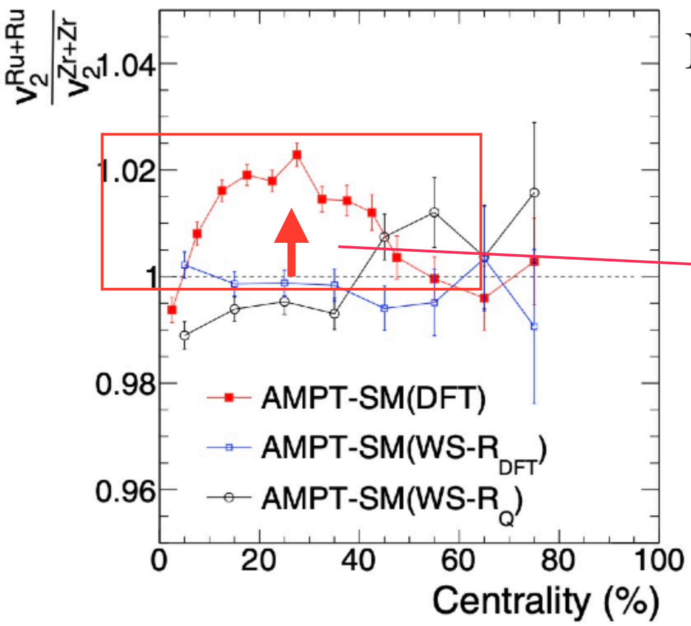

Neutron skin thickness $\Delta r_{np} \equiv \sqrt{\langle r_n^2 \rangle} - \sqrt{\langle r_p^2 \rangle}$

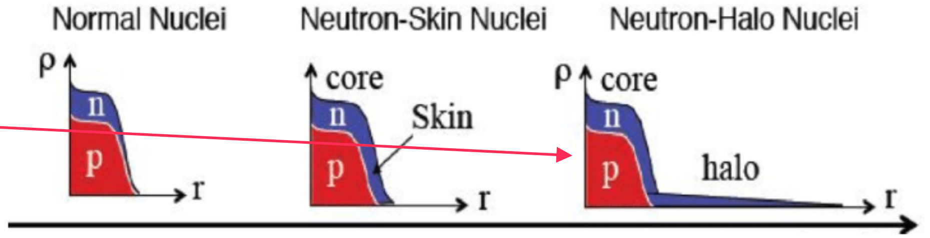

Normal Nuclei	Neutron-Skin Nuclei	Neutron-Halo Nuclei
$R_n = R_p$	$R_n > R_p$	$R_n = R_p$
$a_n = a_p$	$a_n = a_p$	$a_n > a_p$

$$\rho = \frac{\rho_0}{1 + \exp\left[\frac{r - R}{a}\right]}$$

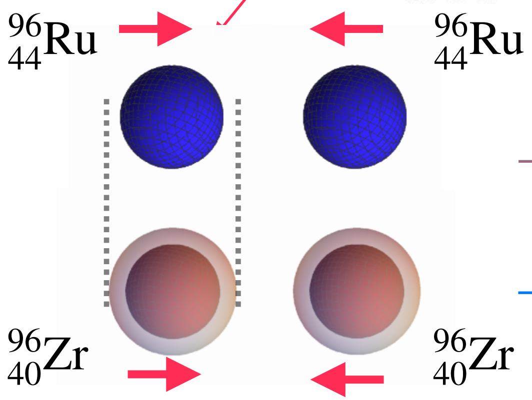

→ Smaller r, larger density → Larger N_{ch} and $\langle p_T \rangle$

→ Larger r, smaller density → Smaller N_{ch} and $\langle p_T \rangle$

HJX, et.al., PRL121, 022301 (2018)
H. Li, HJX, et.al., PRC98, 054907 (2018)
HJX, et.al., PLB819, 136453 (2021)

The STAR isobar data demonstrate **thick halo-type neutron skin in Zr,** consistent with **DFT** (energy density functional theory) calculations

IV. Probing the neutron structure with relativistic isobaric collisions

Relativistic heavy ion collisions

Woods-Saxon distributions

$$\rho(r) = \frac{\rho_0}{1 + \exp[(r - R)/a]}$$

$$R = R_0\,[1+\beta_2 Y_2^0(\theta)+\beta_4 Y_4^0(\theta)]$$

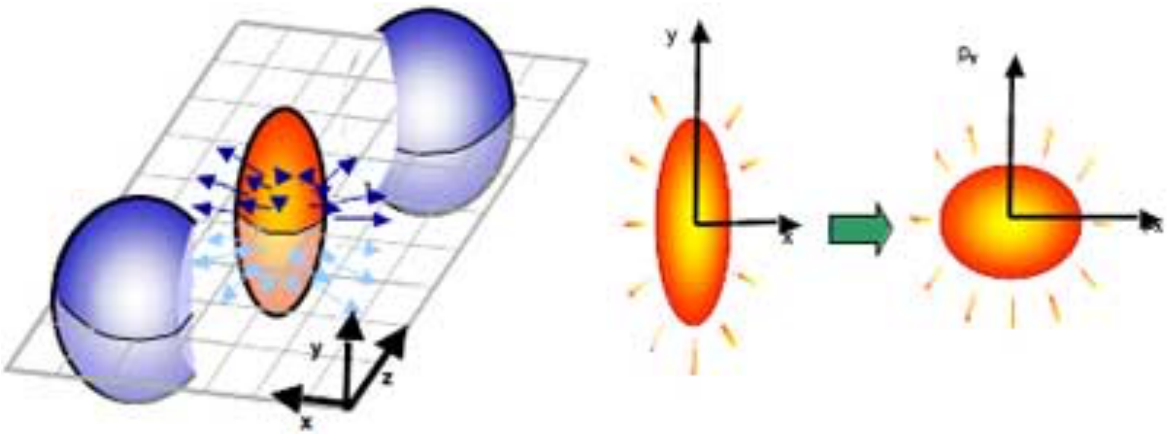

Anisotropic flow,
Flow fluctuations
HBT,
....

Bulk properties of QGP medium: $\eta/s, \zeta/s, \ldots$

Initial geometry

Final observables

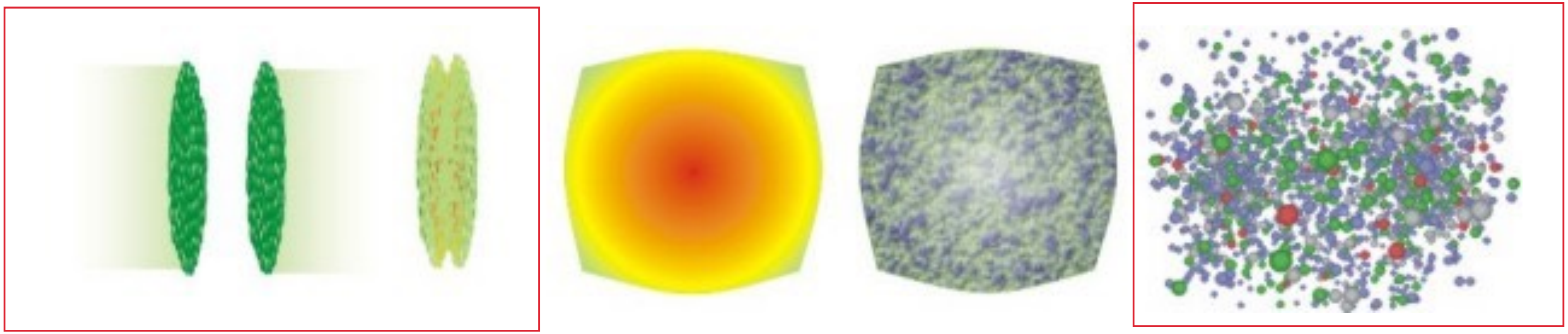

Current status of neutron skin measurements

PREX-2 Collaboration, PRL126, 172502(2021); B. Reed, et.al., PRL126, 172503(2021)

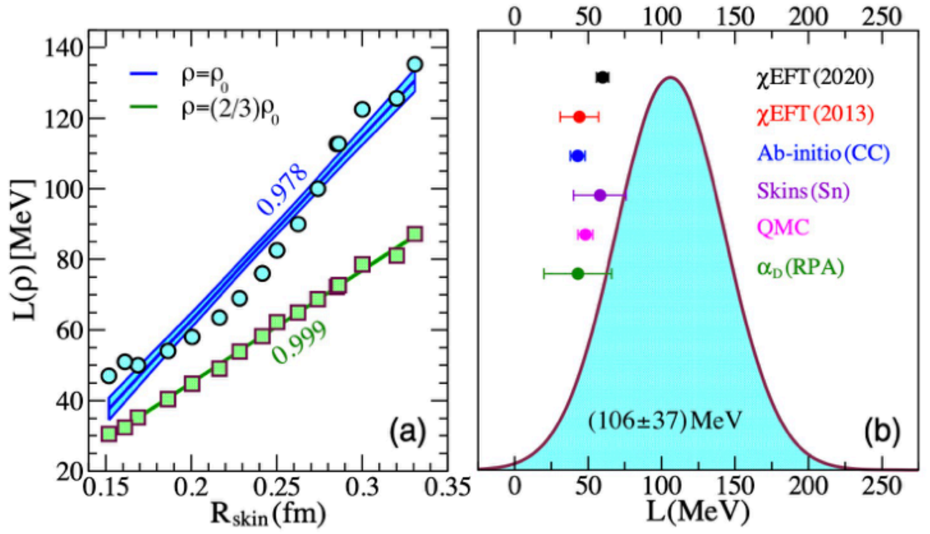

FIG. 1. Left: slope of the symmetry energy at nuclear saturation density ρ_0 (blue upper line) and at $(2/3)\rho_0$ (green lower line) as a function of $R^{208}_{\rm skin}$. The numbers next to the lines denote values for the correlation coefficients. Right: Gaussian probability distribution for the slope of the symmetry energy $L = L(\rho_0)$ inferred by combining the linear correlation in the left figure with the recently reported PREX-2 limit. The six error bars are constraints on L obtained by using different theoretical approaches [14,19–25].

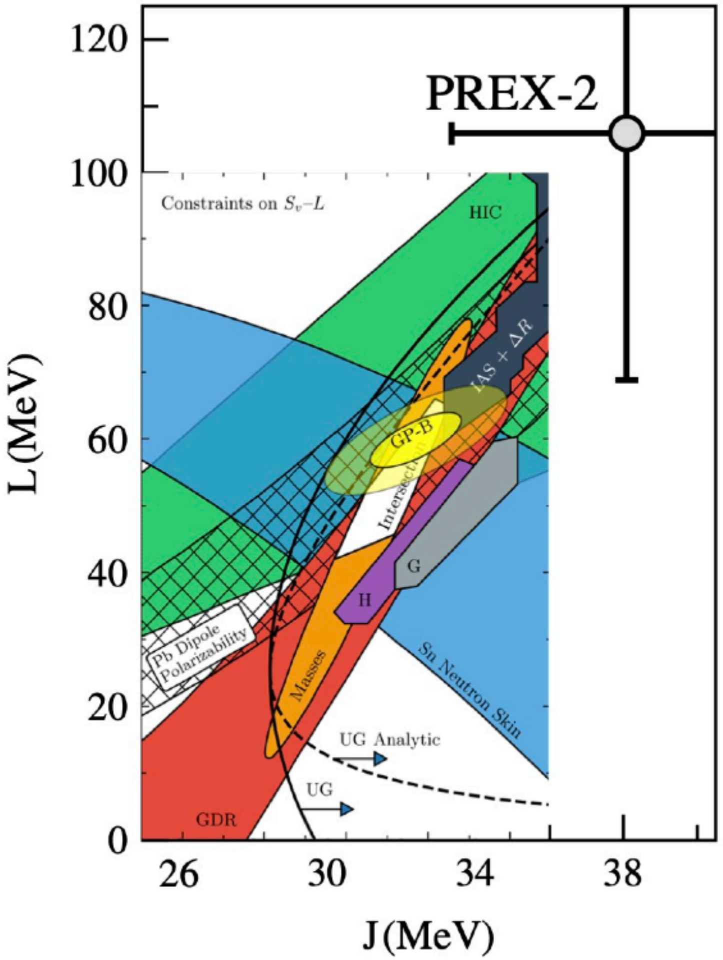

$$\Delta r_{\rm np}^{\rm Pb} = (0.284 \pm 0.071)\ \text{fm}$$

$$L(\rho_0) = (106 \pm 37)\ \text{MeV}$$

$$L(\rho_c) = (71.5 \pm 22.6)\ \text{MeV}$$

This PREX-2 result favors a large neutron skin thickness and symmetry energy slope parameter, at tension with existing experimental data and theoretical analyses.

Neutron skin and nuclear symmetry energy

H. Li, HJX, et.al., PRL125, 222301(2020)

SHF: Standard Skyrme-Hartree-Fock (SHF) model
eSHF: Extended SHF model

$$E(\rho,\delta) = E_0(\rho) + E_{\rm sym}(\rho)\delta^2 + O(\delta^4)$$

$$\rho = \rho_n + \rho_p; \ \ \delta = \frac{\rho_n - \rho_p}{\rho}$$

$$L(\rho_c) = 3\rho_c \left[\frac{dE_{\rm sym}(\rho)}{d\rho}\right]_{\rho=\rho_c} ; \ \ \rho_c \simeq 0.11 {\rm fm}^{-3}$$

Z. Zhang, PRC94, 064326(2016)

$$\begin{aligned} v_{i,j} &= t_0(1+x_0P_\sigma)\delta(\boldsymbol{r}) + \frac{1}{6}t_3(1+x_3P_\sigma)\rho^\alpha(\boldsymbol{R})\delta(\boldsymbol{r}) \\ &+ \frac{1}{2}t_1(1+x_1P_\sigma)[K'^2\delta(\boldsymbol{r}) + \delta(\boldsymbol{r})K^2] \\ &+ t_2(1+x_2P_\sigma)\boldsymbol{K}'\cdot\delta(\boldsymbol{r})\boldsymbol{K} \\ &\boxed{+ \frac{1}{2}t_4(1+x_4P_\sigma)[K'^2\delta(\boldsymbol{r})\rho(\boldsymbol{R}) + \rho(\boldsymbol{R})\delta(\boldsymbol{r})K^2] \\ + t_5(1+x_5P_\sigma)\boldsymbol{K}'\cdot\rho(\boldsymbol{R})\delta(\boldsymbol{r})\boldsymbol{K} \quad \text{Extended}} \\ &+ iW_0(\boldsymbol{\sigma}_i + \boldsymbol{\sigma}_j)\cdot[\boldsymbol{K}'\times\delta(\boldsymbol{r})\boldsymbol{K}], \qquad (4) \end{aligned}$$

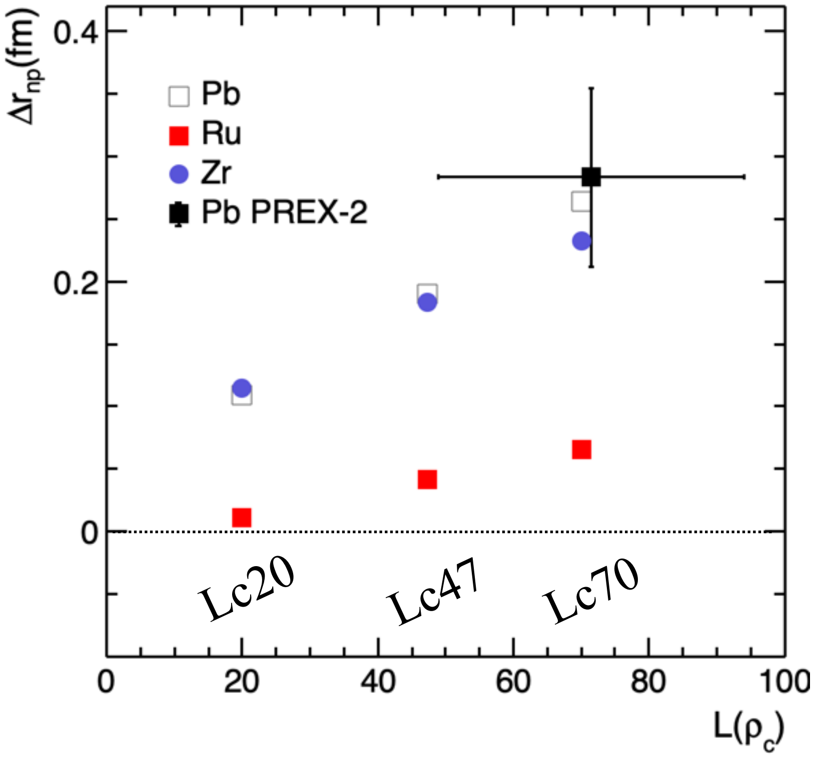

	$L(\rho_c)$	$L(\rho_0)$	^{96}Zr r_n	^{96}Zr r_p	^{96}Zr $\Delta r_{\rm np}$	^{96}Ru r_n	^{96}Ru r_p	^{96}Ru $\Delta r_{\rm np}$	^{208}Pb $\Delta r_{\rm np}$
Lc20	20	13.1	4.386	4.27	0.115	4.327	4.316	0.011	0.109
Lc47	47.3	55.7	4.449	4.267	0.183	4.360	4.319	0.042	0.190
Lc70	70	90.0	4.494	4.262	0.232	4.385	4.32	0.066	0.264
SLy4	42.7	46.0	4.432	4.271	0.161	4.356	4.327	0.030	0.160

Method I: multiplicity distribution ratio

H. Li, HJX, et.al., PRL125, 222301(2020)

Lc47: DFT calculations using data from terrestrial nuclear experiments and astrophysical observations.
Y. Zhou, L. Chen, Z. Zhang, PRD99, 121301R(2021)

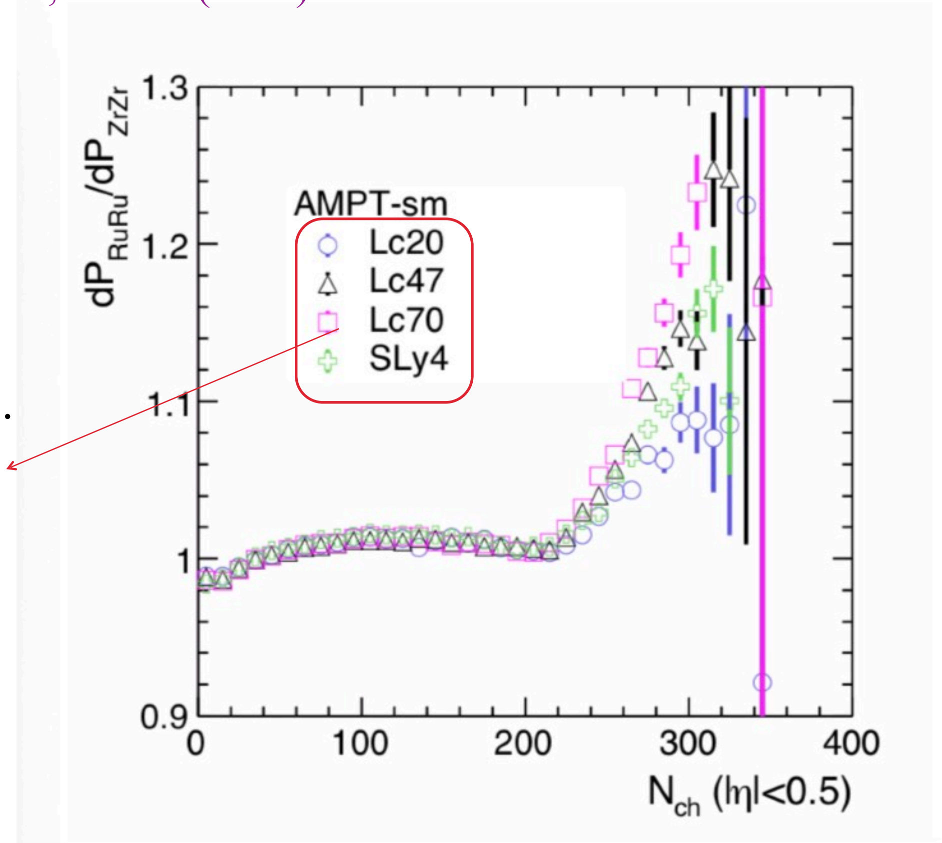

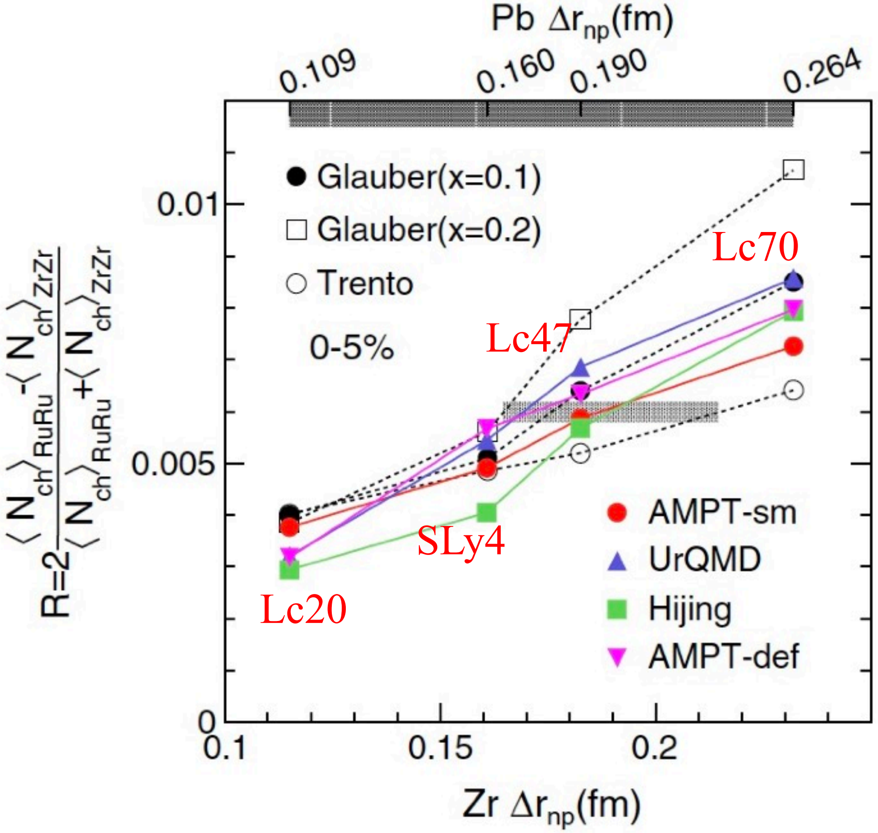

- The ratio of N_{ch} distributions highlight the differences
- To quantify the differences, we use the R observable of N_{ch} at top 5% centrality.
- R is a relative measure, **much of experimental effects cancel**
- Deformation has an effect on the tail. Quantitative investigation underway.

Method II: mean p_T ratio

HJX, et.al, arXiv:2111.14812

b=0 fm

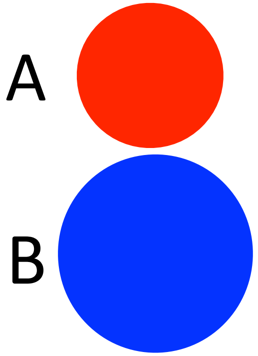

A → smaller $R_\perp$ → larger N_{ch} and $\langle p_T \rangle$

B → Larger $R_\perp$ → Smaller N_{ch} and $\langle p_T \rangle$)

$$R(\langle p_T \rangle) \propto R(d_\perp) \propto 1/R(\langle \sqrt{r^2} \rangle)$$

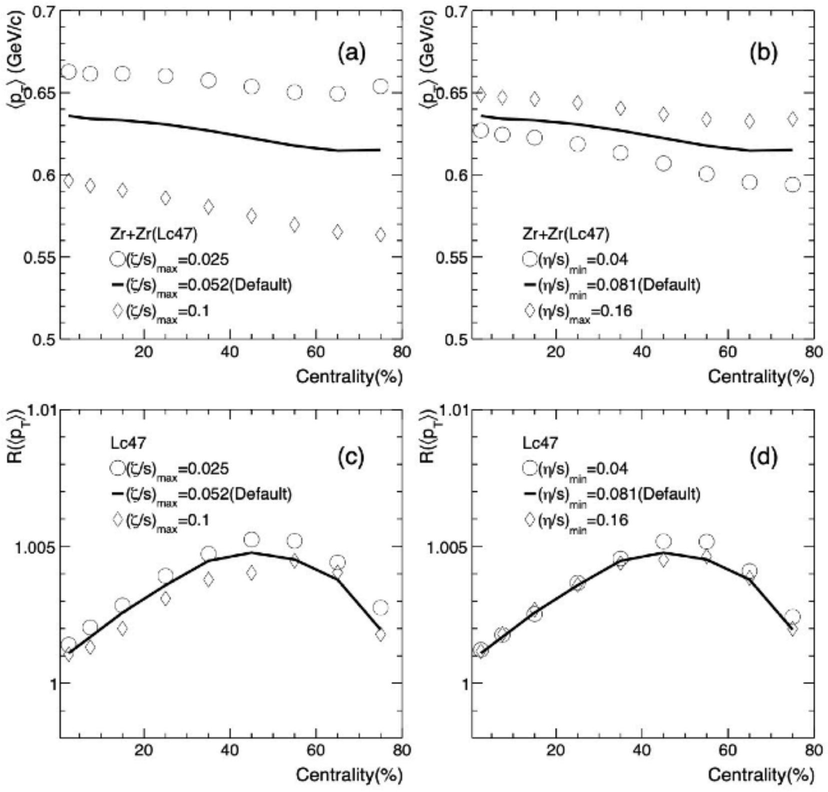

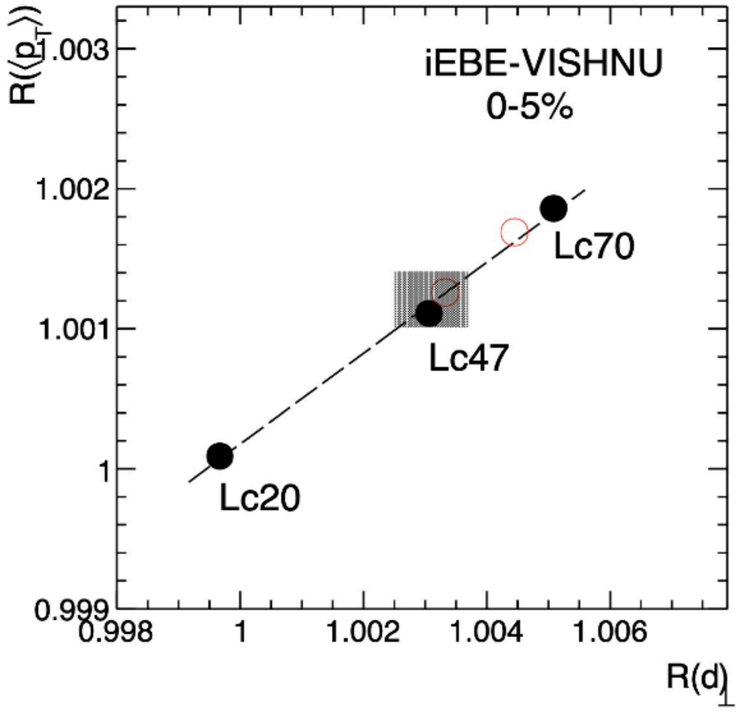

The $R(\langle p_T \rangle)$ is inversely proportional to nuclear size ratio in most central collisions.

Method III: net-charge ratio in very peripheral collisions

HJX, et.al., PRC105, L011901 (2022)

For the colliding nuclei with large neutron skin thickness

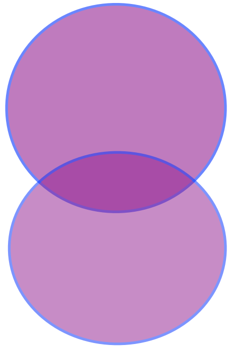

→ more n+n collisions at most peripheral collisions → Less participant charges, thus less final net-charges

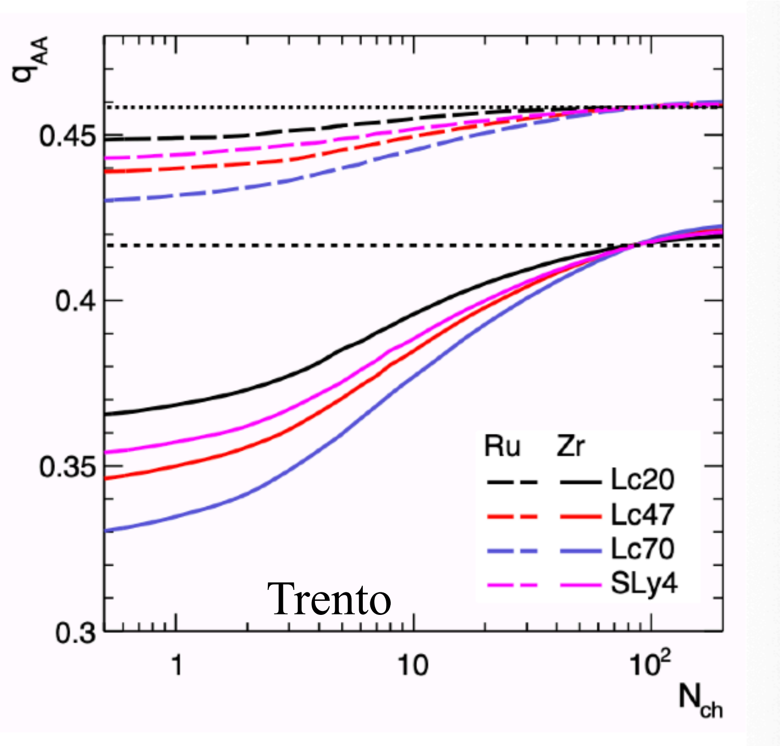

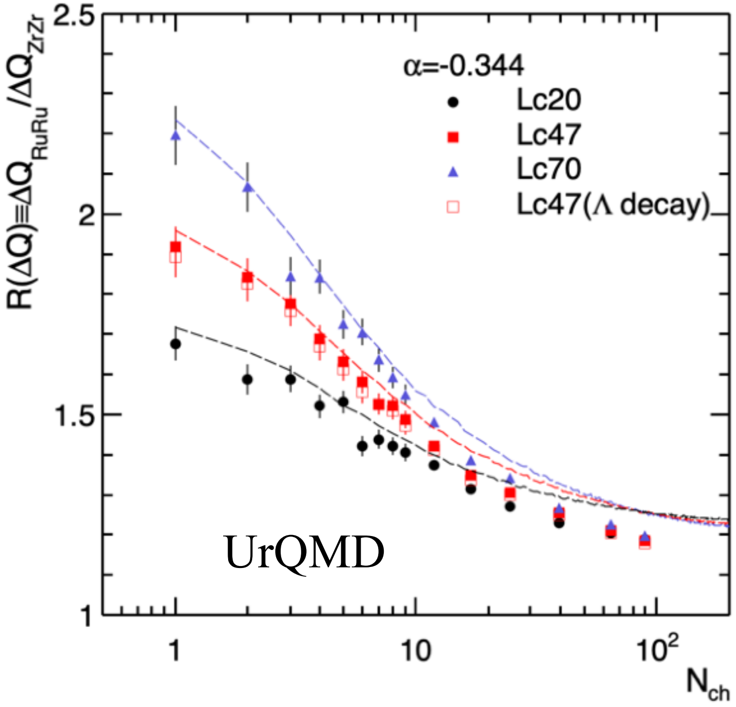

The curves are calculated by superimposition assumption

$$R(\Delta Q) = \frac{q_{RuRu} + \alpha/(1-\alpha)}{q_{ZrZr} + \alpha/(1-\alpha)}$$

where $q_{RuRu/ZrZr}$ are the fraction of protons among the participant nucleons, obtained by the Trento model.

α is the ΔQ ratio in nn to pp interaction:

Pytha: $\alpha = -0.352$

Hijing: $\alpha = -0.389$

UrQMD: $\alpha = -0.344$

Haojie Xu

STAR measurements

Compare to world wide data

HJX(STAR)[18], QM2022

State-of-the-art **spherical** DFT with eSHF nuclear potential

Zhang, Chen, PRC94, 064326 (2016)

- Multiplicity ratio:

$$L(\rho_c) = 53.8 \pm 1.7 \pm 7.8 \text{ MeV}$$

$$L(\rho) = 65.4 \pm 2.1 \pm 12.1 \text{ MeV}$$

$$\Delta r_{\text{np,Zr}} = 0.195 \pm 0.019 \text{ fm}$$

$$\Delta r_{\text{np,Ru}} = 0.051 \pm 0.009 \text{ fm}$$

- $\langle p_T \rangle$ ratio:

$$L(\rho_c) = 56.8 \pm 0.4 \pm 10.4 \text{ MeV}$$

$$L(\rho) = 69.8 \pm 0.7 \pm 16.0 \text{ MeV}$$

$$\Delta r_{\text{np,Zr}} = 0.202 \pm 0.024 \text{ fm}$$

$$\Delta r_{\text{np,Ru}} = 0.052 \pm 0.012 \text{ fm}$$

B. Li, et.al Universe 7, 182 (2021)

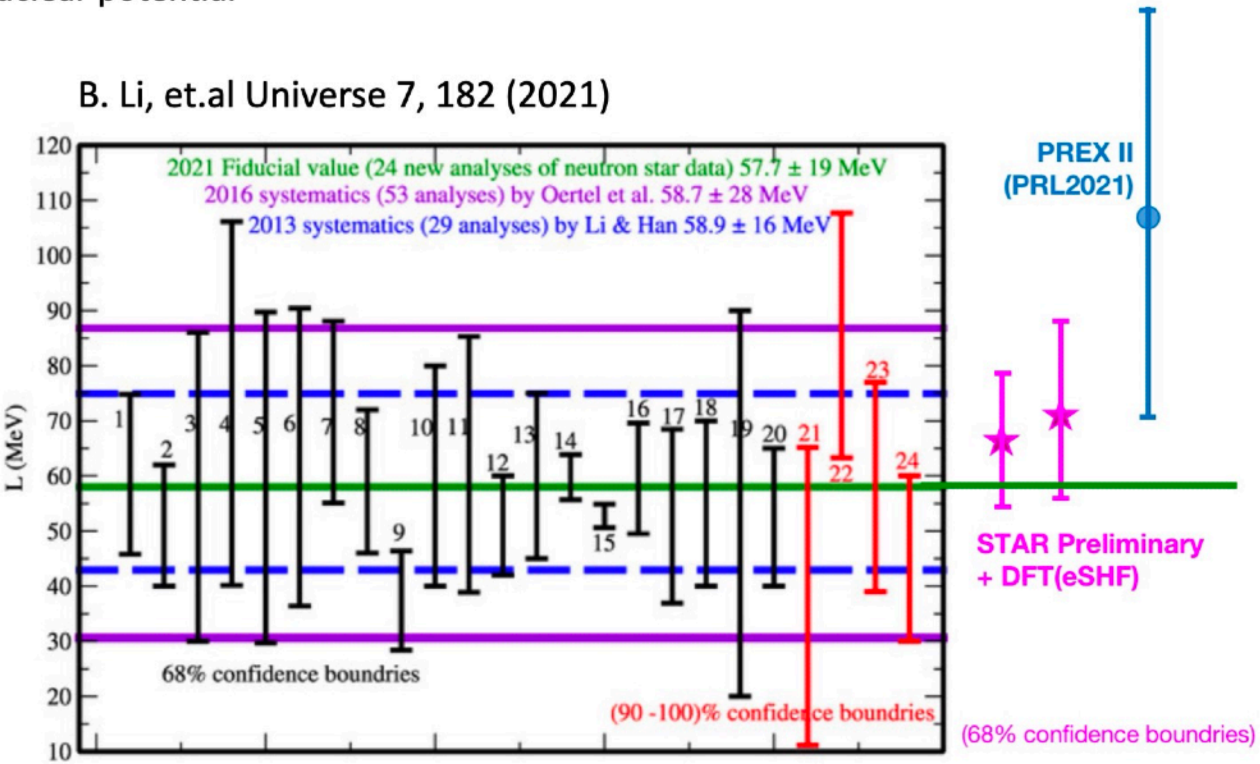

Consistent with world wide data with good precision

Nuclear deformation

STAR, PRC105, 014901 (2022)
C. Zhang, J. Jia, PRL128, 022301(2022)

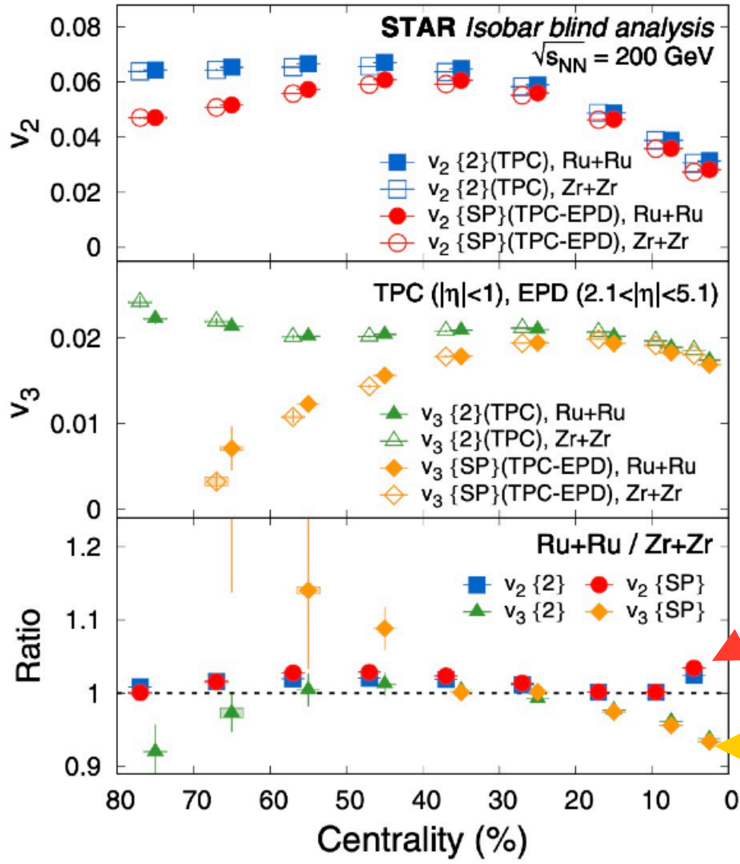

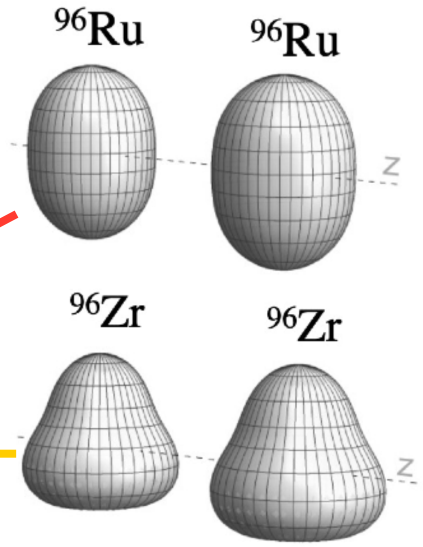

Sizable v_2 and v_3 ratios in central collisions indicate **shape difference between isobars**

Importance of initial fluctuation

STAR, Isobar, PRC105, 014901(2022)
C. Zhang, J. Jia, PRL128, 022301(2022)

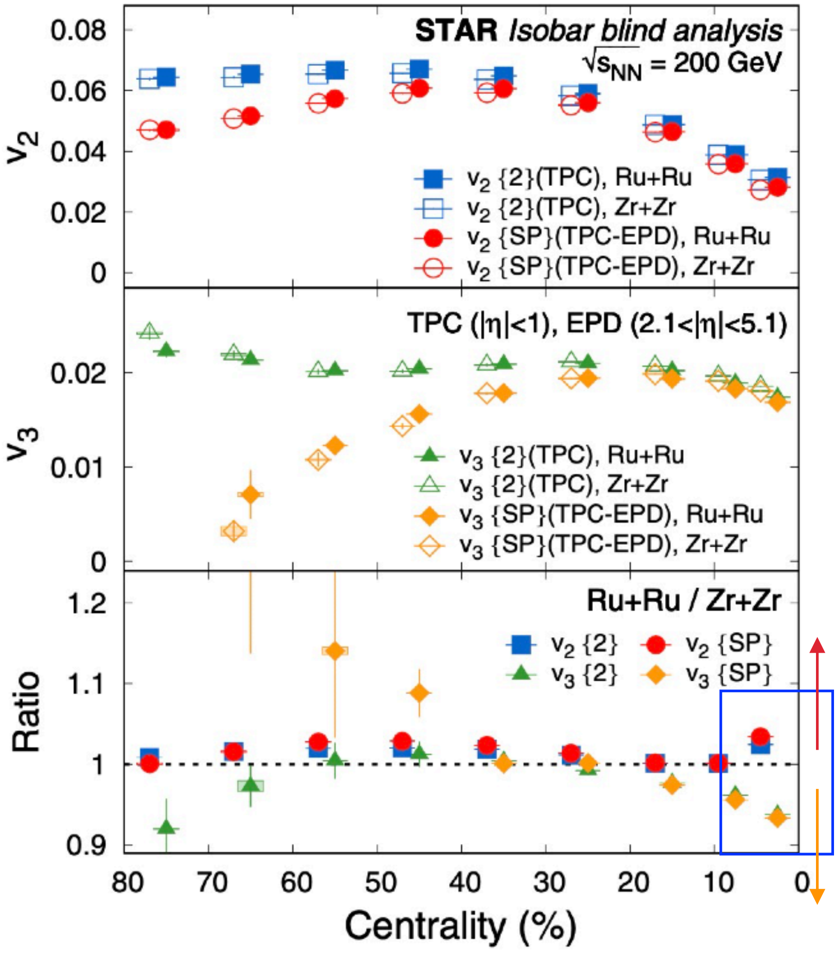

Sizable v_2 and v_3 ratios in most central collisions may indicate shape difference in isobars.

J. Wang, HJX, et.al, in preparation

^{96}Ru				^{96}Zr			
ρ_0	R	a	β_2	ρ_0	R	a	β_3
0.159	5.093	0.488	0.00	0.163	5.022	0.538	0.00
0.159	5.090	0.473	0.16	0.163	5.016	0.527	0.16

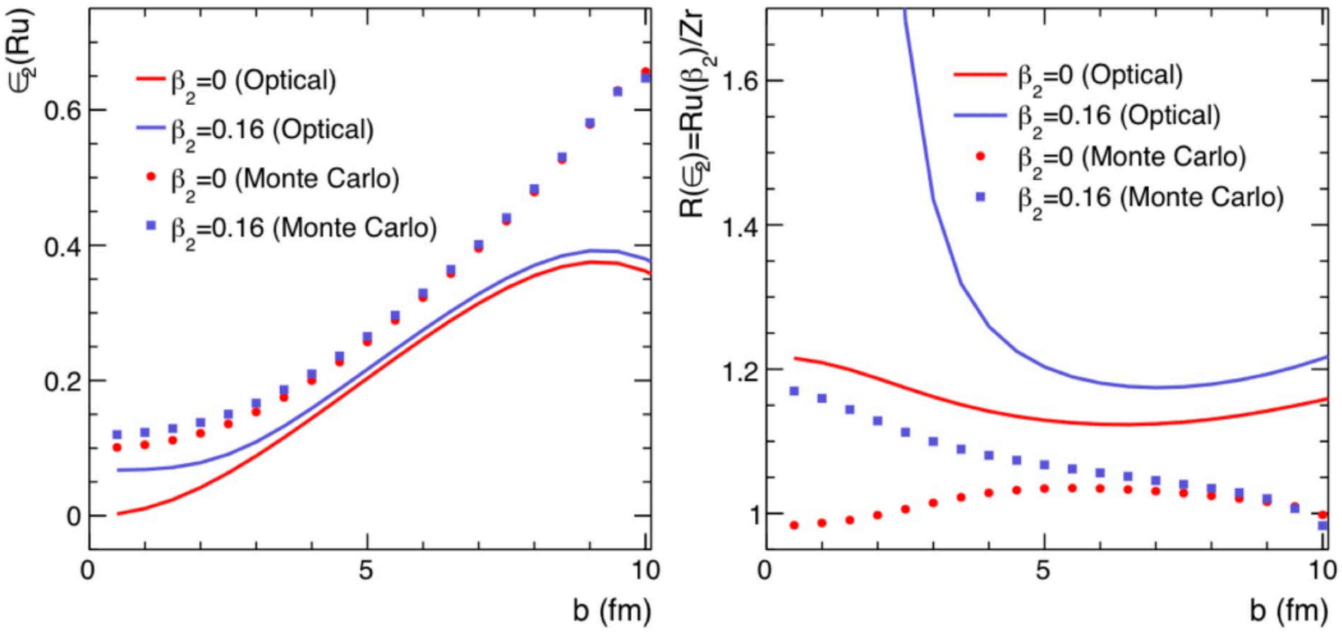

The initial fluctuation significant dilute the geometry differences from nuclear densities

Fluctuation modeling is important.

Importance of initial fluctuation

G. Giacalone, et.al, arXiv:2111.02908

J. Wang, et.al, in preparation

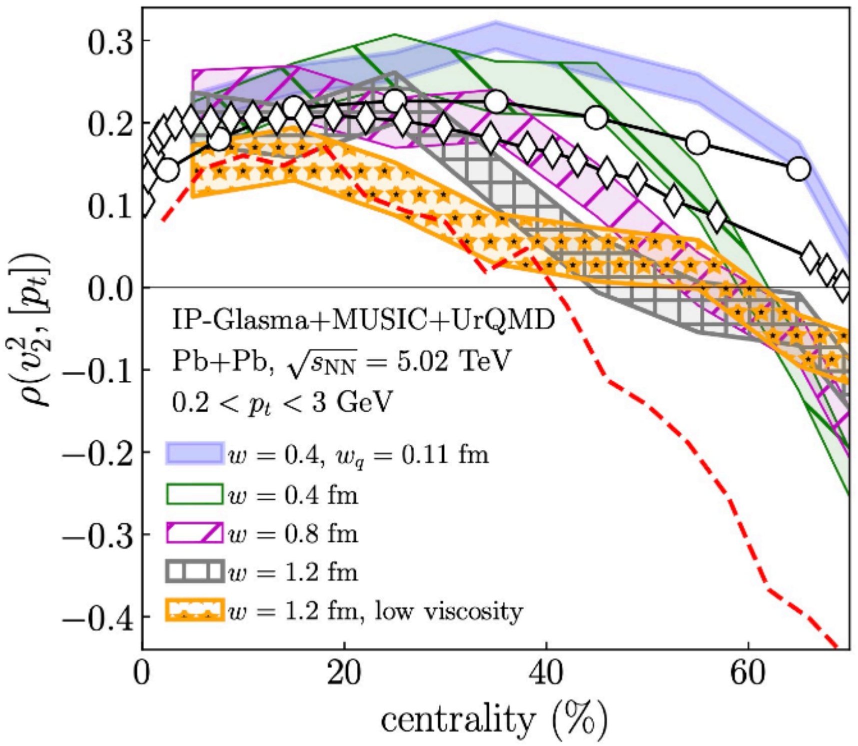

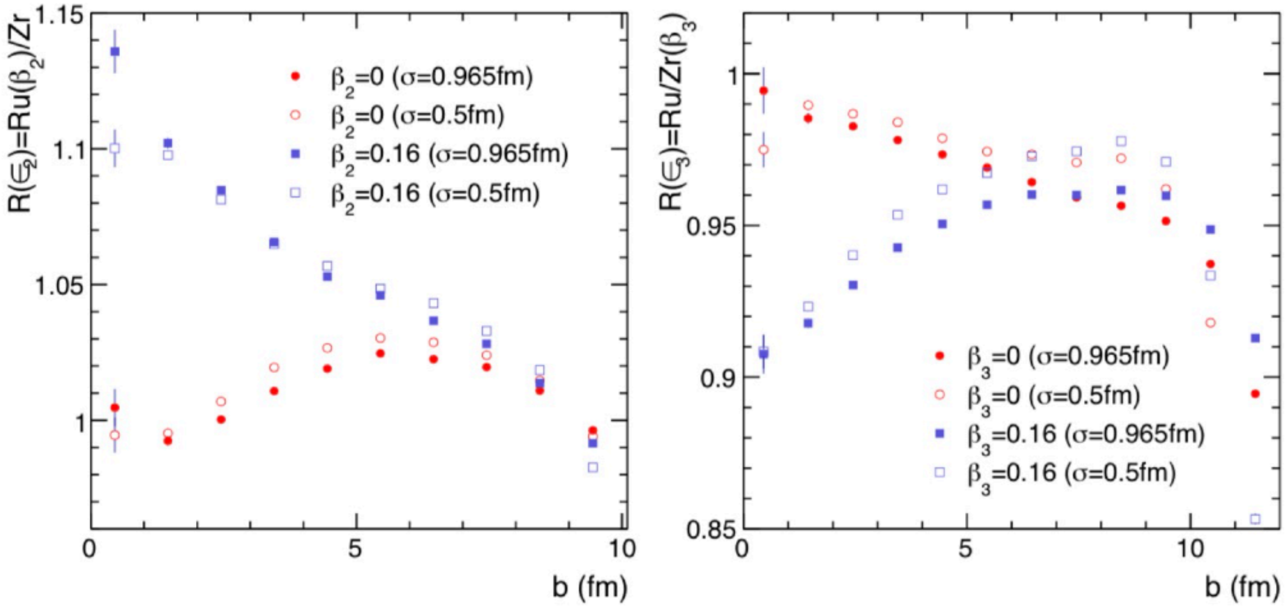

$$\rho_n \equiv \rho(v_n^2, [p_t]) = \frac{\langle \delta v_n^2 \delta [p_t] \rangle}{\sqrt{\langle (\delta v_n^2)^2 \rangle \langle (\delta [p_t])^2 \rangle}},$$

The nucleon width parameter has sizable contributions to the third order eccentricity (anisotropic flow) differences.

Asymmetric cumulant

S. Zhao, et.al, arXiv:2204.02387

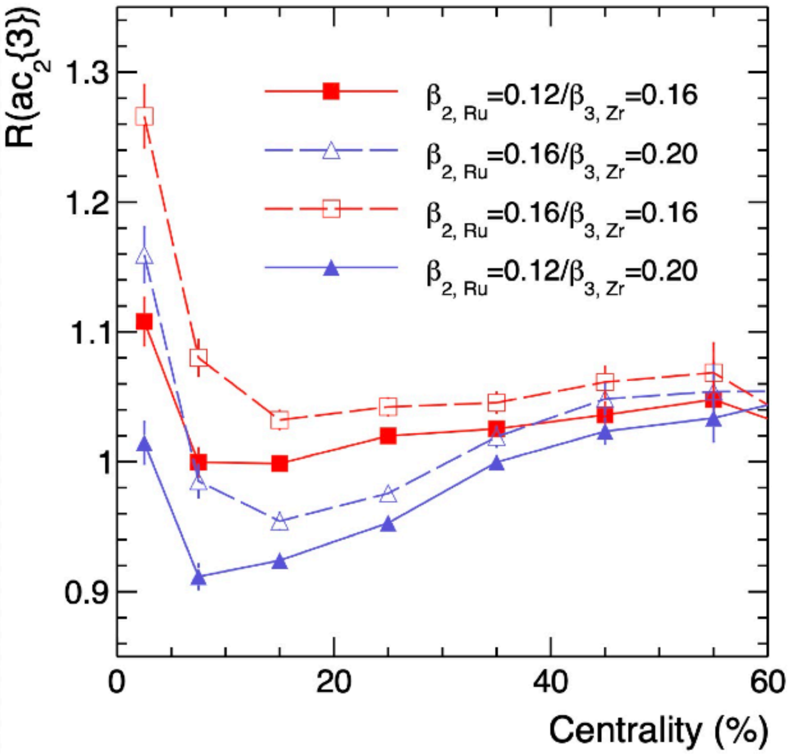

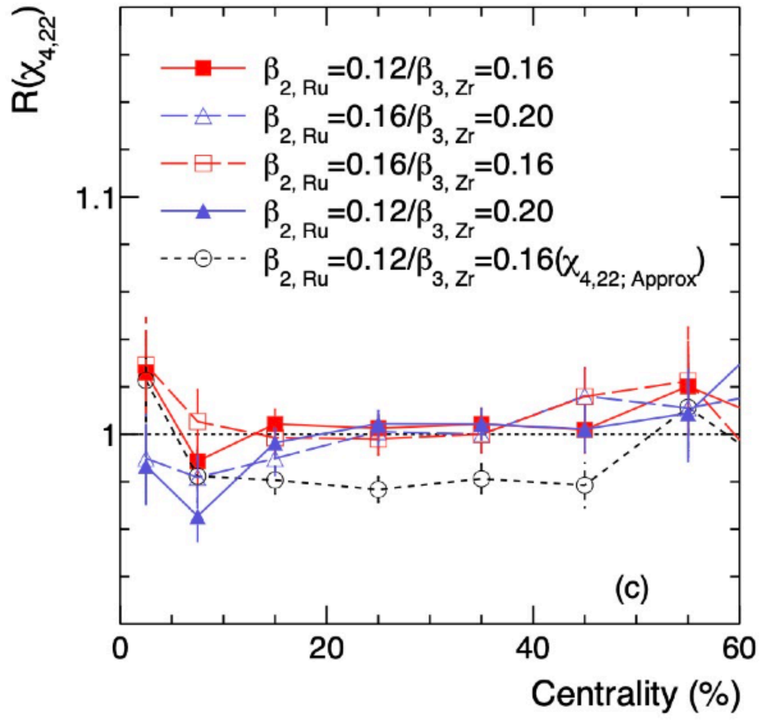

Non-linear coefficient: $\langle \chi_{4,22} \rangle = \dfrac{\mathrm{ac}_2\{3\}}{\langle v_2^4 \rangle}$

$$\mathrm{ac}_2\{3\} \equiv \langle\langle e^{i(2\varphi_1+2\varphi_2-4\varphi_3)}\rangle\rangle = \langle v_2^2 v_4 \cos 4(\Psi_2 - \Psi_4)\rangle$$

Expectation: $\dfrac{\mathrm{ac}_2\{3\}_{\mathrm{RuRu}}}{\mathrm{ac}_2\{3\}_{\mathrm{ZrZr}}} = \dfrac{\chi_{4,22}^{\mathrm{RuRu}}}{\chi_{4,22}^{\mathrm{ZrZr}}} \dfrac{\langle v_2^4 \rangle_{\mathrm{RuRu}}}{\langle v_2^4 \rangle_{\mathrm{ZrZr}}}$

V. SUMMARY

- Although current data are too weak to be definitive, the SP/PP method points out a potentially very important direction for CME search.
- The isobar density distributions are **crucial for the CME search**.
    - Sizable v_2 and multiplicity distribution differences at non-central collisions
    - Large enhancement of multiplicity differences and flow differences at most central collisions
- Ultra-relativistic isobar collisions can be used to **probe the isobar structure**, e.g. the neutron skin type, thickness, and nuclear deformation.
    - Multiplicity distribution ratio; Mean p_T ratio; Net charge ratio;
    - Flow observables, asymmetric cumulants

Thank you for your attention!

Haojie Xu(徐浩洁)

Huzhou University(湖州师范学院)